DIPLOMARBEIT

Design of an electron beam ion source for experiments with ultrafast timing resolution using SIMION simulations

zur Erlangung des akademischen Grades

Diplom-Ingenieurin

im Rahmen des Studiums

Technische Physik

eingereicht von

Johanna FRIES
Matrikelnummer 01425904

Ausgeführt am
Institut für Angewandte Physik
der Fakultät für Physik
der Technischen Universität Wien

unter der Anleitung von
Ass.Prof. Dr. Richard A. WILHELM
und
Univ.-Prof. Dr. Friedrich AUMAYR

Wien, 18. Oktober 2020

Johanna Fries	Richard A. Wilhelm	Friedrich Aumayr

Abstract

Within the time4ions project, an ion source will be constructed to generate ultrashort ion pulses. With these pulses, different processes during the ion-solid interaction will be investigated in real time. Until now, only the final states after an ion-solid interaction can be investigated without the opportunity to study the dynamics of the processes directly. Because these interactions occur on many different time scales, only processes in a range larger than some nanoseconds can be observed. With ultrashort ion pulses of $\ll 10$ picoseconds it will be enabled to investigate interaction processes in an even lower time regime, aiming to reach the sub-picosecond range.

The objective of this master's thesis is to perform first simulations for the time4ions project. Therefore, the established electron beam ion source (EBIS) concept is used and adapted to simulate ion trajectories with the help of SIMION simulations. Starting from the design of a commercial EBIS, several parts are adapted within the computer-aided design (CAD) software SOLIDWORKS. This results in different simulation geometries aiming for an optimum time4ions setup. These adapted geometries, given in form of a CAD drawing are furthermore implemented into SIMION and act as a basis for particle trajectory simulations. Within SIMION, the different particle properties are defined, including the ion species and charge state, the ions' starting positions and a velocity distribution. The calculation of the velocity vectors includes a contribution coming from the electron impact ionisation occurring in an EBIS and a Maxwell Boltzmann distribution for the ambient temperature.

Evaluating the recorded simulation data, the ion pulse width of the simulated ion beam is determined within a Python program. The data is filtered with respect to the ion energy similar to an electrostatic energy analyser in the experimental realisation of the setup. Applying the mentioned methods, various parameters such as the electrode voltages, the recording positions, the temperature and the electric field are varied and analysed with the aim of a decreasing ion pulse width. Using an optimised parameter set, ion pulse widths in the range of a few picoseconds could be achieved.

Kurzfassung

Das time4ions Projekt soll es zukünftig möglich machen, ultrakurze Ionenpulse zu erzeugen und mit deren Hilfe Ionisationsprozesse auf sehr kleinen Zeitskalen zu untersuchen. Dafür wird eine Ionenquelle konstruiert, um damit verschiedene Prozesse, die während einer Ionen-Festkörper-Wechselwirkung passieren, in Echtzeit zu analysieren. Bisher ist es möglich, nur die Zustände nach einer solchen Wechselwirkung zu betrachten und daraus Rückschlüsse auf die stattgefundenen Prozesse zu ziehen, nicht aber derartige Wechselwirkungen direkt zu untersuchen. Da diese auf unterschiedlichen Zeitskalen passieren, können auch nur gewisse Prozesse mit herkömmlichen Ionenstrahlen aufgelöst werden, nämlich jene die nicht unter dem Nanosekunden-Bereich stattfinden. Mithilfe der generierten ultrakurzen Ionenpulse ($\ll 10$ Picosekunden) soll es nun möglich werden, auch kleinere Zeitskalen bis unter den Picosekunden-Bereich direkt zu untersuchen.

Das Ziel dieser Masterarbeit ist es, erste Simulationen für das time4ions Projekt durchzuführen. Dafür wird das bekannte Konzept einer Elektronenstoßionenquelle (EBIS) verwendet und auch adaptiert, um Ionentrajektorien mit der Simulationssoftware SIMION zu simulieren. Als Basis dient ein kommerziell verfügbares Design einer Elektronenstoßionenquelle, welches im Laufe der Arbeit modifiziert wird. Nachdem einige Teile innerhalb der computerunterstützten Software SOLIDWORKS bearbeitet wurden, können verschiedenen Simulationsgeometrien für einen optimalen Aufbau analysiert werden. Diese Geometrien können in SIMION geladen werden und fungieren als Simulationsvolumen für die Simulation der Trajektorien. Innerhalb der Simulationssoftware SIMION werden die verschiedenen Teilcheneigenschaften festgelegt, zum Beispiel die Ionensorte und der Ladungszustand, die Startpositionen und die Geschwindigkeitsvektoren der Teilchen. Die Berechnung der Geschwindigkeit setzt sich aus zwei Teilen zusammen: zum einen aus dem Beitrag der Elektronenstoßionisation, die in einer EBIS stattfindet, und zum anderen aus einer Maxwell-Boltzmann-Verteilung, die die Temperatur im experimentellen Aufbau repräsentieren soll. Innerhalb der Datenauswertung mit Python wird schlussendlich die Pulsbreite der simulierten Ionen bestimmt. Die Daten werden derart gefiltert, um einen experimentell eingesetzten elektrostatischen Energieanalysator nachzuahmen. Um möglichst niedrige Pulsbreiten zu erhalten, werden unter Verwendung der oben genannten Methodik die verschiedenen Parameter, wie zum Beispiel die Elektrodenspannungen, die Position für die Datenerfassung, Temperatur und elektrisches Feld variiert, um die Ionenpulsbreiten zu minimieren. Zudem wurde ein optimierter Parametersatz verwendet, womit Pulsbreiten im Picosekunden-Bereich erreicht werden konnten.

Contents

1 State of the Art and Motivation

The interaction of ions with solid surfaces has been investigated for several decades. The research has an enormous field of application, including semiconductor technology [1], the astrophysics sector [2], particle therapy [3] and nuclear fusion [4], to name but a few. New insights in the involved processes with ion beams will thus strongly help to improve the currently used techniques and applications. This does not just lead to a large impact on fundamental research in physics, but also in many technological and industrial areas.
When an ion hits a surface, many different processes occur starting with the ion interacting with the surface atoms before actually reaching the surface itself. After the ion impact, a collision cascade is formed leading to sputtering, desorption, electron emission, recrystallisation, and many more. These processes happen on a broad range of time scales, ranging from the sub-femtosecond (fs) for charge exchange to the microsecond regime for ad-atom production. The timescales for the involved processes are shown in figure 1.1. So far, many of these processes are still unexplored in terms of time resolution, because the investigation of interaction processes below the nanosecond (ns) range cannot be observed in real time. Conventional experiments with ion beams can only access the final state, i.e. after the projectile interacted with the target (e.g. with ion beam spectroscopy or surface microscopy). Additional investigation in the time range between approximately 10^{-16} s to 10^{-15} s was and is still performed in experiments using two-dimensional (2D) materials [5, 6]. This time range can be accessed through acceleration of the ions to high kinetic energies and transmission through a thin sample. Hence, the interaction time of projectile and target can be minimised to the sub-fs regime.

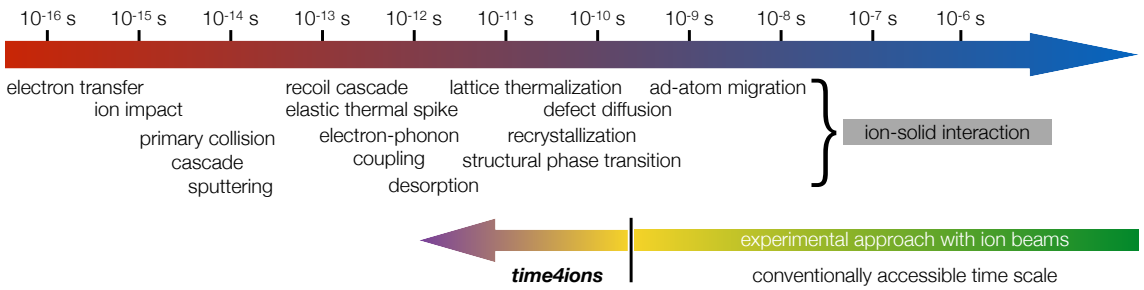

Figure 1.1: Timescale for ion-solid interaction processes.

Furthermore, the dynamics have been simulated mainly using Molecular Dynamics (MD) and Binary Collision Approximation (BCA) codes [7–9]. However, these simulations include

approximations, e.g. the neglect of multi-body interaction potentials.
To be able to observe the time evolution of interaction processes in an experiment, a new method will be developed addressing time evolution of ion impact through a target. The time4ions project aims for an experimental observation of the interaction dynamics in real time. Developing an ion source with a pulse width and timing precision in the (sub-)picosecond (ps) regime to resolve ion scattering processes in the sub-ns and sub-ps range is the key objective. The project will also allow refining the resolution of time of flight spectroscopy and measuring the energy (loss) of ions in the non-equilibrium state for the first time.
To know how to generate ultrashort ion pulses, the following sections shall give a step-by-step introduction in the field of the ionisation processes in general, where they can be applied and how pulsed ion beams can be formed, motivating a time resoled ion-surface-interaction experiment.

1.1 Ionisation processes

Ionisation processes always include the emission or capture of electrons from/to atoms or molecules. Here, positively charged ions are concerned as final state of the process. Ions can be formed, for example, via electron impact ionisation or photoionisation [10].

Photoionisation

When a neutral atom A absorbs electromagnetic radiation in form of a photon $h\nu$, an electron is released exceeding the vacuum level and a positively charged atom is formed

$$h\nu + A \rightarrow A^+ + e^-, \tag{1.1}$$

on the condition that the photon energy exceeds the ionisation energy E_{ion}. The excess energy is released as kinetic energy E_{kin} to the photoelectron and ion

$$h\nu - E_{ion} = E^e_{kin} + E^{ion}_{kin}. \tag{1.2}$$

Thus, whether the ionisation proceeds, depends on the photon energy, i.e. on the frequency ν [11]. Under intensive photon radiation, e.g. by using a pulsed laser with more than $\sim 10^{14} \frac{W}{cm^2}$ per pulse, even two or more photons can be absorbed leading to double or multiple photoionisation, respectively [10].
L'Huillier *et al.* [12] presented the first experimental findings concerning multiply charged ions emerging from the interaction of an intense laser with atoms. In recent years, deeper understanding in multi-photon ionisation was gained, e.g. in combination with the usage of intense ultrashort laser pulses [13, 14].

Electron impact ionisation

One of the most important types of atomic collision processes to generate ions is the electron impact ionisation. The inelastic three - body problem can be described via

$$e^- + A \rightarrow e^- + A^+ + e^-, \tag{1.3}$$

where a neutral atom is separated into an ion and an electron via electron impact [10]. Figure 1.2 shows a schematic of the electron impact ionisation.

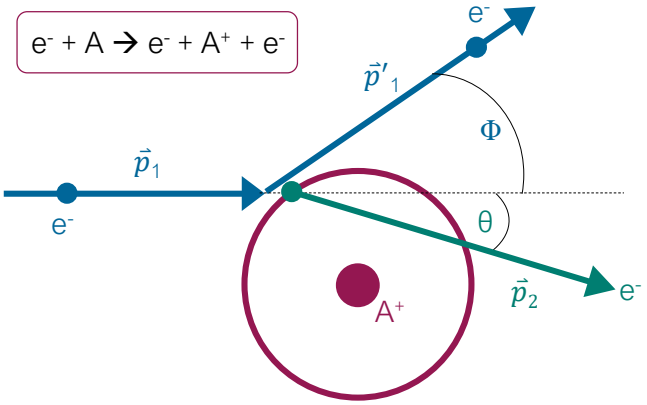

Figure 1.2: Schematic of the electron impact ionisation process.

The cross section for the electron impact ionisation (EII) yields

$$\sigma_{\mathrm{EII}} = \mathrm{R}^2\pi \approx 10^{-17} - 10^{-16}\,\mathrm{cm}^2 \tag{1.4}$$

with R being the screening radius for various ion species. For higher energies, the electron impact ionisation cross section decreases [10, 15, 16].
Considering the simplest atom, Lohmann *et al.* [17] discovered the momentum distribution for the hydrogen ground state ionisation as independent of the total input energy. Years later, McCarthy *et al.* [18] further reported on electron momentum spectroscopy for, *inter alia*, hydrogen. The momentum density (differential cross section $\frac{\mathrm{d}\sigma}{\mathrm{d}\Omega}$) is displayed in figure 1.3 in dependence of the recoil ion momentum. The ion recoil momentum p is defined by the electron momentum before the collision minus the momenta of the scattered and released electrons (non-coplanar symmetric (e, 2e) technique)

$$|\vec{\mathrm{p}}| = |\vec{\mathrm{p}}_1| - |\vec{\mathrm{p}}'_1| - |\vec{\mathrm{p}}_2|. \tag{1.5}$$

Using this particular experimental technique, the outgoing electrons are observed with the same energy and are emitted at a fixed polar angle of 45°. The azimuth angle and the angle

for the free electron-electron collision vary [17]. The cross section for the electron impact of the target atom was measured as a function of the energy and momentum of the incident and the two outgoing electrons. For a detailed description of the experimental setup of a non-coplanar symmetric coincidence spectrometer see [19].

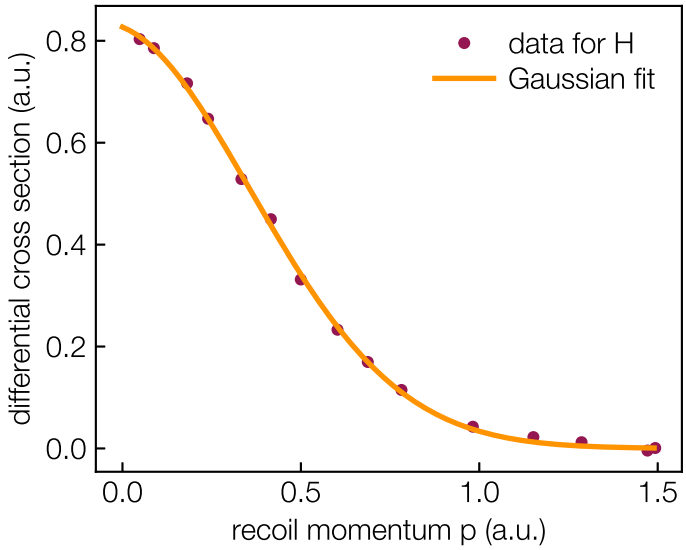

Figure 1.3: Momentum profile for atomic hydrogen as a function of the recoil ion momentum p in atomic units [17]. The recoil momentum is independent from the total input energy. Data points are fitted with a Gaussian.

For simplicity, the angular dependence of the recoil momentum is calculated in the elastic scattering regime (cf. section 2.2). The recoil momentum as a function of the electron scattering angle θ is visualised in figure 1.4 and can be interpreted as a more forward directed movement (see small scattering angles in the inset plot) for the scattered electrons. Note, that small ion recoil momenta (<1 a.u.) are largely preferred (cf. figure 1.3). Regarding the mass relation between a hydrogen ion and an electron

$$\frac{m_{e^-}}{m_{ion}} = \frac{1}{1836}, \tag{1.6}$$

the light electrons are hardly scattered, i.e. they fly more or less along the incoming beam axis. In contrast, calculating the ion recoil momentum for different recoil angles Φ (cf. figure 1.5), again a preferred direction can be observed for the ion. The large recoil angles lead to a deflection of the ions perpendicular to the beam axis, as it is shown in the inset plot in figure 1.5.

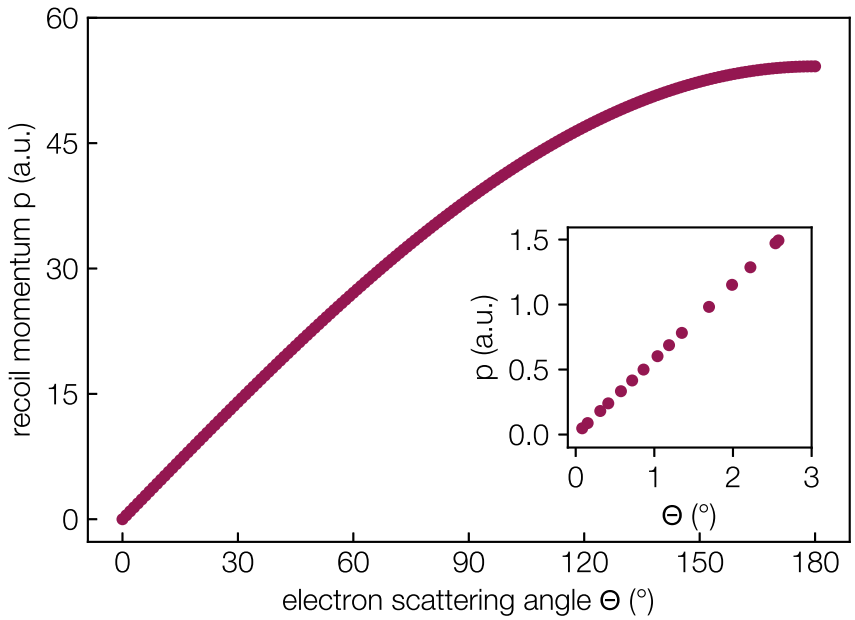

Figure 1.4: Calculated recoil momentum distribution in a.u. for hydrogen as a function of the electron scattering angle. The inset again shows the values for small scattering angles exhibiting high cross sections.

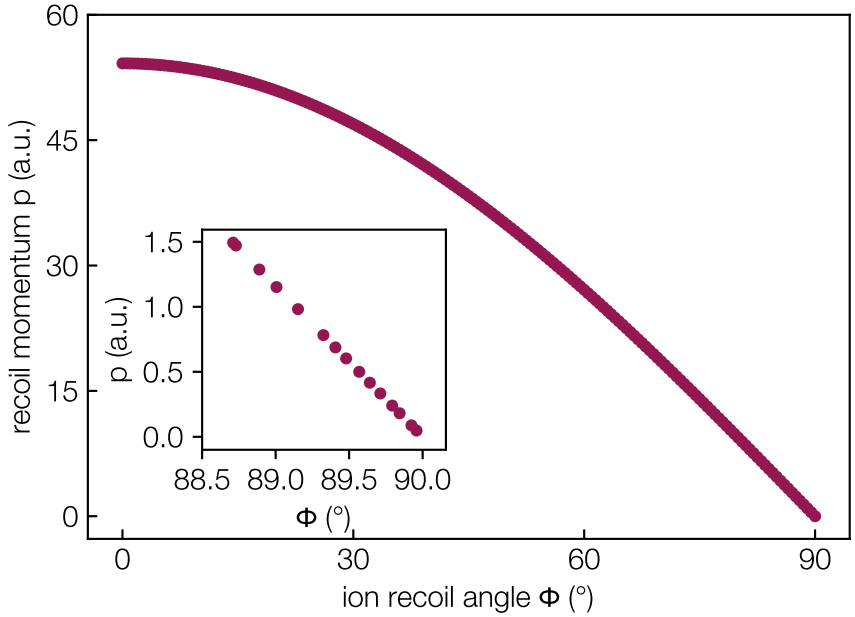

Figure 1.5: Calculated recoil momentum distribution in a.u. for hydrogen in dependence of the ion recoil angle. Note the inset, where momenta with the highest cross section are shown.

The fundamental principles for the formation of ions were discussed. The electron impact ionisation is a process widely used in ion sources, e.g. electron cyclotron resonance ion sources (ECRIS) [20, 21] and electron beam ion sources (EBIS) (cf. section 1.2) for the production of highly charged ions. Representatively the EBIS concept is also important for the work performed in this thesis and is introduced in the following.

1.2 Electron beam ion source

Due to the low probability of achieving highly charged ions with only one electron impact ionisation, a stepwise ionisation is performed in an electron beam ion source (EBIS). Multiple ionisations are realised by keeping the ions trapped in the source for a specific amount of time. In addition, an intense electron beam ensures a higher probability in generating highly charged ions [10]. From a cathode, electrons are extracted and afterwards radially focused by magnetic compression. The magnets lead to a confinement of the electron beam (diameter $\sim 10\,\mu$m) ensuring a high electron density. The electron beam is directed onto the ionisation gas volume within the drift tube section consisting of three electrodes ($U_{D,1}$, $U_{D,2}$, $U_{D,3}$). During ion generation, the potential of the third drift tube $U_{D,3}$ is kept high enough, that the ions are held in a potential trap and are successively ionised. Whether the source is operated in leaky or pulsed mode is defined by $U_{D,3}$. For the leaky mode $U_{D,3} = \text{const.} < U_{D,1}$, where ions with an adequate high kinetic energy can overcome the potential $U_{D,3}$ and leave the drift tube section continuously. When the potential $U_{D,3}$ is switched periodically for a short time, generated highly charged ions can be extracted (pulsed mode). The extraction unit consists of an extraction electrode ($U_{Ex,1}$) and an einzel lens, consisting of three electrodes ($U_{Ex,2}$, $U_{Ex,3}$, $U_{Ex,4}$) to focus the ion beam. $U_{Ex,3}$ is generally kept to a positive potential, while the second and fourth electrodes are grounded. Besides, the electron collector (U_{col}) is installed behind the drift tube section. The final kinetic energy of the ions is defined by $E_{kin} = \frac{m_{ion} v^2}{2} = qU_{D,3}$ in the leaky mode. Additional positive or negative potentials applied to multiple electrostatic lenses extract and form the ion beam [22, 23]. Figure 1.6 shows a schematic of an EBIS generating highly charged ions with a charge state q.

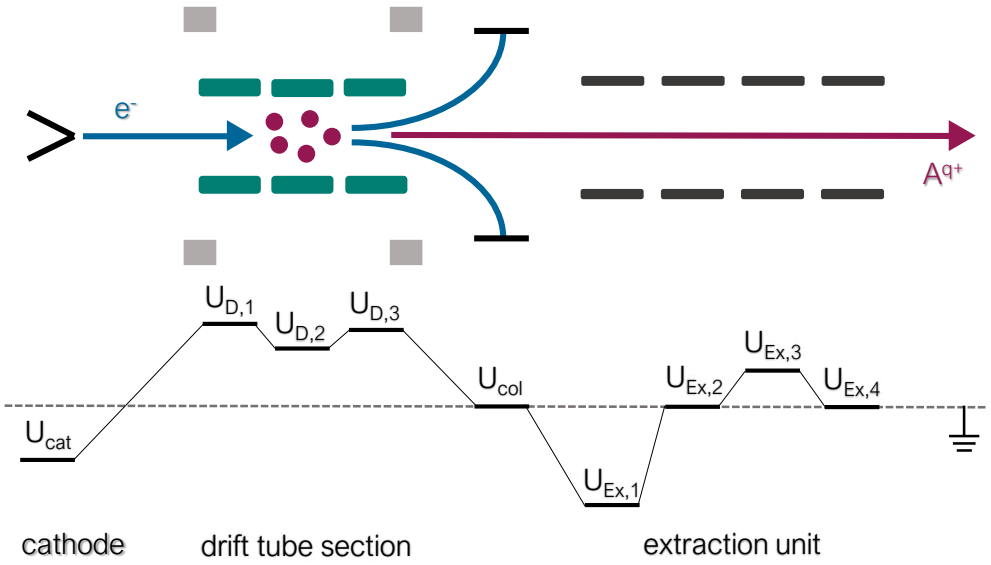

Figure 1.6: Scheme of an electron beam ion source (EBIS) to generate highly charged ions with a charge state q.

1.3 Formation of pulsed ion beams

Being aware of the generation of ion beams, it is of further interest to discuss the formation of pulsed ion beams to perform experiments with high timing resolution and investigate ion-solid interaction processes. Using the EBIS concept, pulsed ion beams can be achieved by operating the source in the pulsed mode (switching $U_{D,3}$). Nevertheless, the pulse length is limited due to the time necessary for switching the drift tube potential.
Another method to generate short ion pulses is via chopping and bunching. At first, a continuous beam is chopped into discrete ion pulses by periodically interrupting the incident beam. This can be realised by a rotating disk with slits acting as a mechanical shutter. However, the motor speed for rotating the disk, the dimensions of the slits and the beam diameter limit the outgoing pulse width. Using deflection plates for chopping an ion beam, takes advantage of the charge of the particles. By switching the plate voltages on and off rapidly, the beam is deflected onto an aperture. Hence, pulse lengths in the range of ns to 100 ps can be achieved. Additionally installing a buncher system allows to minimise the pulse duration to approximately 10 ps [24, 25]. Bunching an ion beam can be implemented by using two electrodes applying zero voltage to the first and positive voltage to the second one (enumerated in the order the ions pass the electrodes). When the chopped beam enters the buncher system, the anterior ions of the pulse are repelled by the positive electrode and thus, delayed. Then, the voltage of the second electrode is set to zero as well, so that the beam does not disperse but a shortened pulse is formed in comparison to the incoming chopped one. The bunched beam can then be extracted. Bunching a beam also involves an increased energy width of the beam,

because the ion pulse is compressed in time. Until now, it is not possible to reduce the pulse width below 10 ps.

Combining photoionisation and an ion optical buncher, Breuers *et al.* [26] developed and introduced a concept for ultrashort ion pulse formation in 2019. Applying the pump-probe technique, commonly used to excite states via a laser pump and analysing the interaction with a time-delayed laser, one laser pulse will be replaced by an ultrashort ion pulse to probe laser excited states and their relaxation dynamics [27]. A superposition of a pulsed supersonic rare gas jet and a pulsed laser beam at orthogonal angles, will lead to photoionisation in the overlapping volume. The generated ions can then be extracted perpendicular to the two incident beams. In addition, the ultrashort ion pulses will be bunched to furthermore interact with the target for a very short time. Simulations predict ultrashort ion pulses of a duration of ps and below by using a low temperature environment in the mK range, more precisely 10 mK, and by keeping very short distances within the future experimental setup. A major issue will be the complex laser cooling system to ensure low temperatures [26].

In parallel with [26], the generation of ultrashort ion pulses is also the key issue of a new project at the Institute of Applied Physics (IAP) at TU Wien. How an ion source has to be designed and which components have to be included, to achieve (sub-)ps ion pulses, ideally 1 ps at first, and observe processes involved in ion-surface interactions will be presented in the following section.

1.4 Experimental setup for ps-ion pulses

In the time4ions project, a technique to generate ultrashort ion pulses will be developed following the concept of an Ultrafast Transmission Electron Microscope (TEM) [28, 29]. Introducing a pump-probe experiment, the electronic and atomic dynamics occurring during the ion-solid-interaction will be investigated using a laser as pump and ion pulses as probe, and later on collisional cascades will be studied by ion-pump laser-probe experiments.
A scheme of the Picosecond Ion beams for Time resolved experiments with Beats of Ultrafast Lasers (PITBUL) setup is shown in figure 1.7. It includes four main sections: a femtosecond laser, an electron beam ion source (EBIS), a delay stage and the pump-probe segment where the ions impinge on the target and are simultaneously synchronised to the laser.
A technique based on laser ionisation is best suitable for generating sub-ps ion pulses. Photoionisation could lead to the desired ion pulses, but demands very high photon energies or densities. Therefore, the laser output power would have to be high and such high power lasers also guaranteeing short pulse durations are not commonly available, costly and not easy to use.
In the pump-probe experiments, a Ti:Sapphire laser produces femtosecond pulses with a

wavelength of $\lambda = 800\,\text{nm}$. This laser (type) is chosen for the indirect laser ionisation (laser-triggered electron impact ionisation) within the project, because it is a very simple and cheap laser system. A semi-transparent mirror ensures that the laser beam is split, using one part for the laser triggered ion source, the other for pumping the target to electronically excited states. By varying the laser power, different excited states in the target atoms can be achieved, i.e. excitation of electrons from the valence to the conduction band or ionisation of electrons leading to plasma states. It may be pointed out that these excited states only have a lifetime in the range of 100 fs to 100 ps [27].

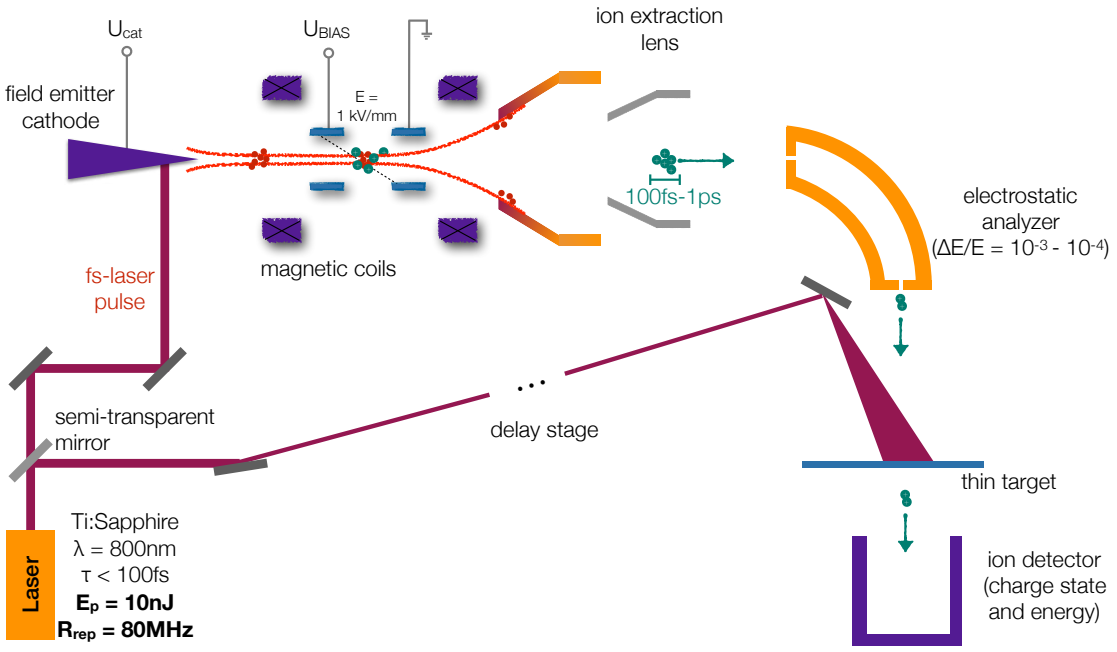

Figure 1.7: Scheme of the PITBUL experimental setup for generating ultrafast ion pulses.

To delay the laser pulse, a time-delay stage [30] can be employed to investigate pump probe delays between $-1\,\text{ns}$ and $+1\,\text{ns}$. Another method leading to a delay between laser and ion pulse is not to use the same laser pulse generated for the ion pulse formation but a later pulse. Here a stable laser oscillator frequency is necessary. However, this approach is beneficial since there is no need to delay for the ion time of flight (TOF) in the order of 10 - 100 ns.
The first mentioned spatially separated fs-laser pulse is directed onto a field emitter cathode to generate ion pulses in an EBIS via indirect laser ionisation. Due to photoemission electron bunches emerge from the tip of the cathode. To minimise the space charge effect, the used laser leads to electron pulses containing not more than 10^3 - 10^4 electrons. Accelerated towards a gas volume in the drift tube unit, the magnetically confined electron pulse leads to the formation of short ion pulses due to electron impact ionisation. For a more detailed description of the EBIS concept, see prior section 1.2. Furthermore, an electric field is applied to the drift tubes to accelerate the ions with different kinetic energies out of the source. To

filter ions with a specific energy, an electrostatic analyser is implemented defining an effective pulse for the pump-probe experiment. Via a small energy window, guaranteeing an energy resolution of $\frac{\Delta E}{E} = 10^{-3} - 10^{-4}$, an effective ionisation volume is defined. This volume must not exceed an axial extension of approximately 100 nm to maintain a timing precision of 1 ps (note that the TOF along 100 nm at the ion energies at hand amount to $\sim$1 ps), defining a well-adjustable potential gradient of about 1 kV/mm in the drift tube section. Within the project, the commercial EBIS concept is adapted to comply with the above-mentioned requirements for the ultrashort ion pulse generation, e.g. in terms of the charge state of produced ions. In an EBIS, highly charged ions can be produced in a three-part drift tube section. Time4ions does not aim in producing highly charged ions, so that the number of tubes can be reduced, additionally reducing flight path. In the future, the experimental setup may also be adapted in a way to directly ionise the gas atoms via the laser and making use of multi-photon ionisation (cf. section 1.1, [26]) if a high power laser becomes available.
The generated and filtered ion pulse in the experiment is directed onto a target. As targets well-established 2D materials are used, in later experiments also solids will be under investigation. After focusing the laser onto a specific area of the target, non-equilibrium states in the target atoms are generated. Afterwards, the laser is defocused slightly and the ion pulse is directed onto the target. The entire experimental setup ensures a synchronisation of the laser and ion pulse at this point. Time dynamics of ionised or excited states of the target atoms under ion impact can be directly determined by investigating the ion energy (loss) and charge state in dependence of the pump-probe delay. In this case the ion serves as probe.
Within the time4ions experiment, various ion species, ion energies and target materials can be applied.
To sum up, in order to investigate the dynamics of at least some ion-solid interaction processes, ion pulses with a pulse length and timing accuracy in the sub-ps range are necessary. Therefore, the experimental setup has to be installed in a very compact way to keep the electron and further ion beam divergence low and to ensure a short time of flight of the involved particles. Thus, first simulations for this completely new ultrafast ion source shall be performed, including drift tube section, extraction unit and electrostatic analyser, motivating the present study.

2 Methods

The following chapter summarises the methodology used to create a simulation geometry within SOLIDWORKS, implement the particles conditions and run the simulation in SIMION. The procedure to evaluate the recorded data is described including the calculation of the ion pulse width being the quantity of interest in this thesis. The last section states inaccuracies of the presented methods.

2.1 SOLIDWORKS

For the simulation of ion trajectories, the geometry for the ions have to be defined. The goal of this thesis is to simulate ion trajectories in an electron beam ion source (EBIS). The particles will be observed from their point of origin until they reach the end of the ion source. Therefore, the three-dimensional computer-aided design (CAD) software SOLIDWORKS [31] is used to design the ion source. Starting with a commercial EBIS [32], the CAD drawings can be modified according to dimensions of individual parts as well as adding or removing components to or from the CAD drawing.
As a basis for the simulations, the used EBIS includes three drift tubes and an ion extraction system with four electrostatic lenses. For simplicity reasons only these parts are implemented in my simulations. Ion source components such as the cathode and magnets are entirely neglected in this thesis. To determine the spatial boundaries for the simulation volume, a hollow cylinder is placed around the drift tube and extraction system. The reduction of components will also help to reduce time within the SIMION refining process, which will be explained in the following section 2.2.
In figure 2.1 a CAD drawing of the used EBIS can be seen. The left part consists of three drift tubes, the right part forms the extraction system. In more detail the extraction unit consists of four lenses electrically separated by insulators. The first lens indicates the ion extraction lens, the remaining three build an einzel lens to focus the ion beam. In the first instance, all extraction lenses are grounded to focus on the drift tube section. The outer boarders of the volume are radially defined by the cylinder placed around the drift tube and extraction units. The cylindrical coating is subsequently grounded to the same extent as a chamber wall in a vacuum facility. Regarding the EBIS geometry, the ion pulse widths are mostly determined by the drift tube section. There, parts of the ions' properties, such as the velocity due to the drift tube bias voltage and the length of the drift tubes itself are defined. Within this first step of the EBIS geometry construction in SOLIDWORKS the spatial dimensions, i.e.

length of and distance between the drift tubes, are varied. The distances between the different electrodes are particularly important for the electrostatics in the experiment. When applying high voltages it is necessary to keep the distances between the parts as small as possible to avoid influences of external electric fields (cf. section 3.1). Once the parts in SOLIDWORKS are defined, the assembly is saved as STL files. This file format can then be read by SIMION.

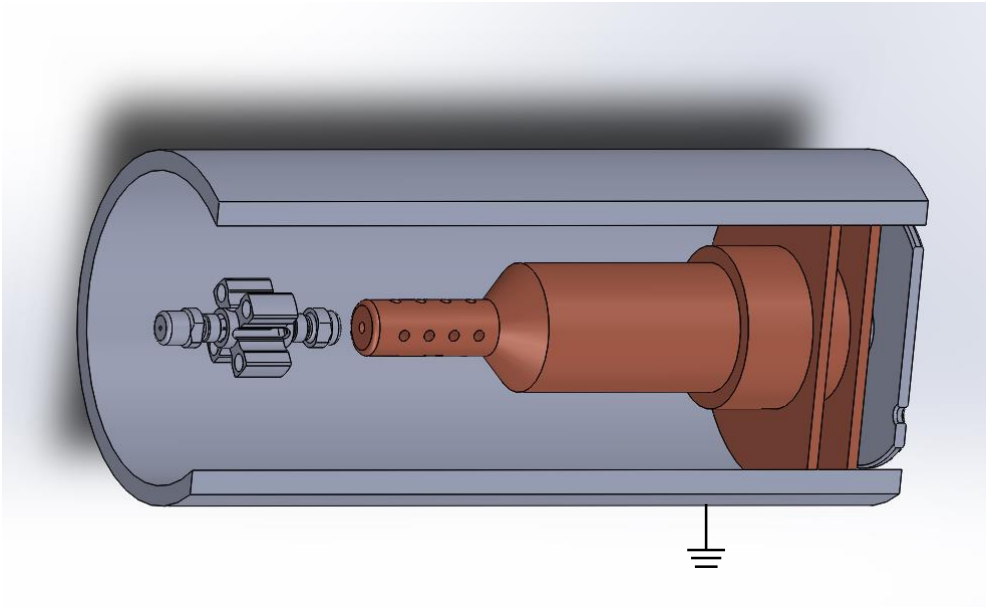

Figure 2.1: CAD drawing of an electron beam ion source (EBIS) with three drift tubes in grey (left) and the extraction unit in brown (right). The EBIS parts are surrounded by a grounded cylinder to define the total simulation volume (grey). All dimensions are based on a commercially available EBIS from DREEBIT GmbH, Germany [32].

2.2 SIMION

The simulation of particles within this thesis is performed using the ion trajectory simulation program SIMION [33]. With SIMION, well-established particle trajectory simulations have been performed for over 30 years. It is one of the best tools for ion trajectory simulations as it offers a graphical user interface (GUI) and the variety of functions covers the definition of the geometry, user programming, recording the data and visualising the trajectories [33].
The working principle of SIMION is primarily to calculate the electric fields of a given geometry and simulate trajectories of charged particles. SIMION includes many more features such as magnetic fields and collisional effects, for example. Starting with the definition of the configuration of the electrodes, voltages are applied and the charged particles are given their initial properties.
In the following, the different steps for the simulation of the ion trajectories are presented. Starting with the STL file as an input for the simulation geometry and going over the refine

process, different particles properties as well as voltages of the electrodes are discussed [34].

Read in STL files: grid definition

During the usage of SL Tools, an additional program within SIMION, the STL files created with SOLIDWORKS are read in. An important step here is the definition of the grid and grid cell size, respectively. It defines how well the geometry is spatially resolved, which can indeed influence the determined ion pulse width due to numerical inaccuracies in the end (cf. section 2.4.1). Small cell sizes and hence good resolution would minimise this effect. Therefore, a good trade-off between resolution and used disk space needs to be found, because the finer the grid cell size the larger the output files created by SIMION. A finer grid also has the consequence of a much longer duration of the posterior performed refining process. The grid dimensions used within this thesis are as precise as possible regarding the limitation from the disk space but can lead to small discontinuities in terms of centring of the ion beam. This means that a radial offset of the particles can occur due to the grid definitions. For the used geometries and ion trajectory simulations the coordinates are defined as follows: x and y axis are perpendicular to the beam and z refers to the ion beam axis. Because the design of the EBIS is radially symmetrical, x and y will be denoted as radial coordinates too in the following.

Refine process

After defining the simulation grid, the *potential arrays* (PA) have to be created. In these arrays the information about the electrodes is stored. A potential array therefore defines electrostatic and magnetic fields. In this thesis, only electrostatic information is stored within a potential array. One array refers to one electrostatic electrode of the studied geometry, i.e. the electron beam ion source in my case. To create the potential arrays, the *refine* process has to be performed. Refining means solving the Laplace equation for the electrostatic potential U,

$$\nabla^2 \mathrm{U} = \Delta \mathrm{U} = 0, \tag{2.1}$$

at every point in space, using the electrode array points as boundary conditions. Numerically, SIMION uses finite difference techniques for refining. By using the Laplace equation to define the potentials, space charge effects are not included [34]. Depending on the selected grid cell sizes the refine process can be more or less time-consuming. With the potential arrays created after the refining, large disk space is necessary for the PA files. Out of the PA files (related to one PA for every electrode) a workbench can be created in a next step. The *ion optics workbench* (IOB) includes all arrays and is a 3D rectangular volume where the simulation of the ion trajectories is performed. This means, that the IOB defines the simulation volume. The dimensions within the workbench are indicated in mm. In addition, the workbench coordinate system can be redefined. To ease the operation within SIMION the radial coordinates are shifted from a value defined in the EBIS' CAD drawing to 0 for x and y coordinates of the ion beam positions. The z coordinate already origins at 0 with the used geometry of the

tailor-made EBIS.

Fast Adjust Voltages

In a next step, the voltages of the electrodes of the ion source have to be defined. Within the graphical user interface of SIMION the applied voltages for every electrode in the simulation volume can be viewed and also changed to the desired value in Volts. This allows a determination of the EBIS' drift tube voltages in combination with a desired potential gradient between them.

Here, the distance between two drift tubes (an electrostatic electrode for SIMION) is called $a_{D,1\text{-}D,i}$ with $i = 2{,}3$ in the following. For drift tube 1 and drift tube i, two different voltage values are applied resulting in an electric potential gradient $\frac{dU}{dz}$ given in kV/mm. Within this thesis, a linear potential gradient is primarily desired as mentioned in section 2.1. For example, if the second drift tube is removed in the CAD geometry, the distance will be called $a_{D,1\text{-}D,3}$ with $i = 3$ even though there are only two drift tubes in total. Referring to the geometry with all three drift tubes (G4, cf. table 3.1) the voltage gradient is applied between the first and the second drift tube using $a_{D,1\text{-}D,2}$ as a distance. Here, the same voltage is applied to the second and third tube to guarantee a linear potential gradient $\frac{dU}{dz}$ between 1 and 2. Figure 2.2 shows a scheme for the definition of the electric field including the distance $a_{D,1\text{-}D,i}$ between drift tube 1 and i.

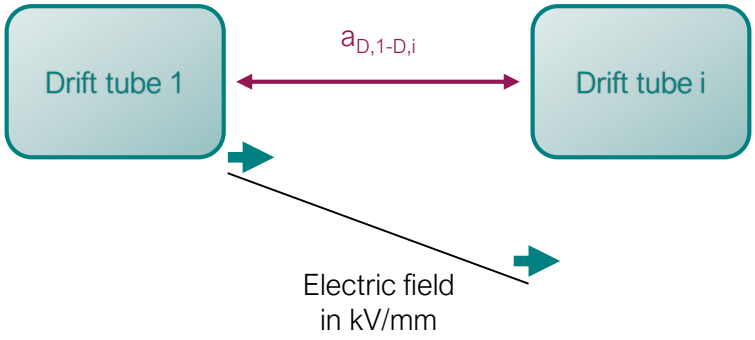

Figure 2.2: Electric field scheme.

Particle definitions

A next step is to set all particle properties including species, charge state, number of particles, time of birth of simulated ions, axial and radial starting conditions and velocity distribution including the temperature. In this thesis, all simulations are made with the same ion species and charge state. The chosen *particle species* is hydrogen in combination with a *charge state* of 1, i.e. only singly charged protons with a mass of $m_{ion} \approx 1$ u are simulated. For good statistics in the data evaluation, it is necessary to keep the *number of particles* high to simulate many ions in a comparatively small volume.

For the *volume of birth* and the spatial origin of the ions the physical background of the electron impact ionisation is used. In the experiment, the electron beam is focused onto a gas volume and as the electrons collide with the hydrogen atoms or molecules, ions are formed through the ionisation process. To reproduce this phenomenon as good as possible a radial extent from the beam axis is added. In a first attempt, an electron beam with a defined radius of 25 μm is assumed. This radial enlargement around the beam axis defines the starting positions of the ions in x and y direction. In addition, the axial origin area of the ion has to be defined. This area is solely defined by the user and is chosen in a way to ensure a minimum pulse width in the end. In general, this area is located between the drift tubes or at the edges of the drift tubes. The radial and axial dimensions are implemented via a cylindrical distribution meaning that the ions are uniformly randomly generated within the defined cylinder (cf. [34]) with a centre at z_{centre} and a length of $l_{cylinder}$. Table 2.1 shows the definitions of the starting position by a cylindrical distribution. The axis of the flying ions is defined as the z direction and the fill argument specifies whether the cylinder is filled with ions or just the edges are used as starting conditions.

Table 2.1: Definition of the starting position of the ions by a cylindrical distribution implemented in the particles' conditions.

position type	cylindrical distribution
centre	(0,0,z_{centre})
axis	(0,0,z)
radius	0.025 mm
length	$l_{cylinder}$
fill	true

Ion velocity calculation

A main part of this thesis was the determination of the ions' conditions in terms of temperature, momentum and velocity, respectively. It should be mentioned here that the following physical quantities are calculated using the laboratory frame of reference. With the help of the programming language LUA [35] a script for the calculation of the ion velocity vector for every single particle was written. This LUA script, in SIMION language termed fly2, includes the physics of the electron impact ionisation as well as the temperature. To guide the reader through the script, table 2.2 describes the input, the actual calculation and the output SIMION uses for simulating the ions.

The basis for the calculation of the velocity distribution is the momentum of the ion

$$\vec{p} = m_{ion} \cdot \vec{v}, \tag{2.2}$$

with the momentum vector $\vec{p}$, the velocity vector $\vec{v}$ and the ion mass m_{ion}, which is set to $m_{ion} = 1836\, m_e$. The electron mass in SI units amounts to $m_e = 9.109 \cdot 10^{-31}$ kg. The approach

is to convert a given momentum distribution (cf. electron impact ionisation in section 1.1) into a velocity distribution and generate the ions in SIMION corresponding to the latter. The momentum distribution results from a superposition of the electron impact ionisation (EII) (according to figure 1.3) and the Maxwell Boltzmann (MB) distribution, which includes the temperature conditions in the ionisation region

$$\vec{v} = \frac{\vec{p}_{EII}}{m_{ion}} + \frac{\vec{p}_{MB}}{m_{ion}}. \tag{2.3}$$

Both momentum inputs are given in atomic units (a.u.) while the temperature is given in Kelvin (K). These momenta are the only values which are not calculated in the fly2 script but are processed. All other quantities for the velocity vector calculation are directly defined or computed within the script for every simulated ion.

Table 2.2: Scheme of particle definitions using a fly2 file in SIMION ion trajectory simulations.

Input

p_{EII} in a.u.
p_{MB} in a.u.

$m_{ion} = 1836 m_e$
$\Phi_{EII} = \Phi_{EII}\ (p_{EII})$
$\Phi_{MB} \in [0,\pi]$ rad

$\alpha_{EII} \in [0,2\pi]$ rad
$\alpha_{MB} \in [0,2\pi]$ rad

Fly2 script

$$\vec{v} = \frac{\vec{p}_{EII}}{m_{ion}} + \frac{\vec{p}_{MB}}{m_{ion}}$$

$$\vec{p}_i = \begin{cases} p_{ix} = p_i \cdot \sin(\Phi_i) \cdot \cos(\alpha_i) \\ p_{iy} = p_i \cdot \sin(\Phi_i) \cdot \sin(\alpha_i) \\ p_{iz} = p_i \cdot \cos(\Phi_i) \end{cases}$$

$i = EII, MB$

Φ_i...elevation angles
α_i...azimuthal angles

Output

velocity vector $\vec{v}$
in mm/μs

The input values for the momenta are gained by the calculation of 10^6 randomly distributed momenta according to the data from Lohmann *et al.* [17] (cf. electron impact ionisation in section 1.1) in conjunction with the Gaussian fit for the data points. The input values for the contribution coming from the Maxwell Boltzmann distribution are also given by Maxwell Boltzmann distributed random numbers for the respective temperature condition.
For the calculation, the ion and electron masses in a.u. are defined globally. Another global variable is the time of birth: According to the assumption of a pulsed electron beam emitted by the cathode of the EBIS, the time where the electron impact ionisation takes place, has a specific period of time of $2 \cdot 10^{-7}\,\mu$s at most (electron pulse width). Because electron im-

pact ionisation can take place randomly distributed within this time, an evenly distributed random number between 0 and $2{\cdot}10^{-7}\,\mu$s is chosen for every single ion, where the ion is created.

For one case of kinetic energy, $E = 30\,\text{keV}$, the propagation time of the electron pulse is estimated in a short excursus according to the time of birth definition. For comparison, the propagation time for the distance between the drift tubes in this case, is discussed at first. The electron velocity v_e is given by

$$v_e = \sqrt{\frac{2E}{m_e}} = 1.027 \cdot 10^8\,\text{m/s} \tag{2.4}$$

with the electron mass m_e. Thus, $t_{e,1}$ defines the time the electron pulse needs to propagate from the end of the first drift tube to the beginning of the second one resulting in a distance to travel of $a_{D,1\text{-}D,2} = 1\,\text{mm}$ (cf. geometry G5 in table 3.1), yielding

$$t_{e,1} = \frac{a_{D,1\text{-}D,2}}{v_e} \simeq 9.735\,\text{ps}. \tag{2.5}$$

In addition, the length which the generated ion pulse (cf. section 2.3) had when forming, is determined. For all ions formed between the two drift tubes, the time of birth is blurred by the additional electron propagation time $t_{e,1}$. However, as we will see, the ions will be filtered according to their energy after their extraction. Only ions within a certain energy window ΔE (cf. figure 2.3) will further be used. The range ΔE is directly linked to a starting position range Δz_{start}. To calculate how long the electron beam propagates through this part, the energy filtered axial position range is assigned to

$$\Delta z_{start} = \max(z_{start}) - \min(z_{start}) = 34.84\,\mu\text{m} \tag{2.6}$$

for the ion pulse width ΔTOF definition and can be seen in figure 2.3. For the calculation of the ion pulse width (see section 2.3) an energy window of $\Delta E = 10\,\text{eV}$ is chosen, resulting in $\Delta\text{TOF} = 135.85\,\text{ps}$ (for $T = 300\,\text{K}$). Now, the time for the electron flying through Δz_{start} can be calculated via

$$t_{e,2} = \frac{\Delta z_{start}}{v_e} = 0.3392\,\text{ps} \simeq 340\,\text{fs}. \tag{2.7}$$

Therefore, the position dependence in terms of the propagating electron pulse in the EBIS is important but in the same order of magnitude as the assumed period of time of 200 fs for time of birth.

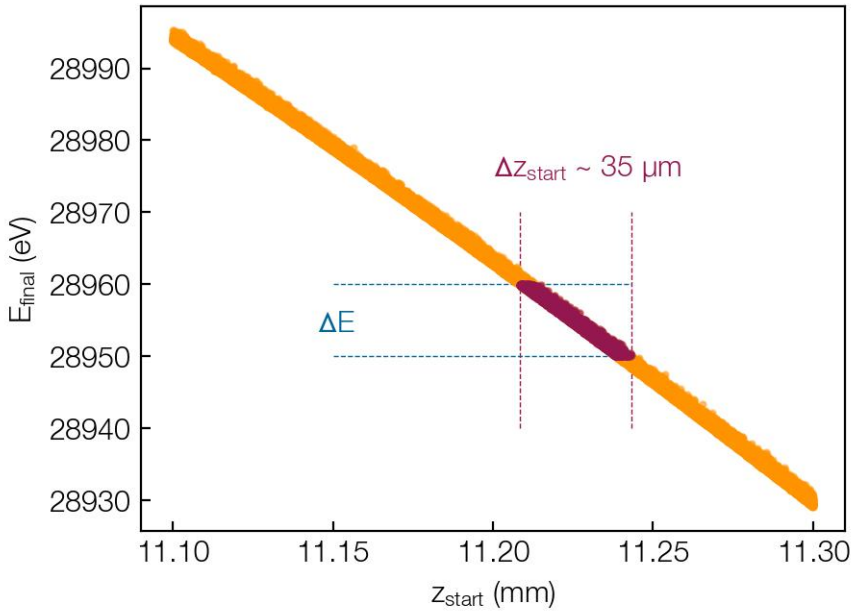

Figure 2.3: Final energy E_{final} in dependence of axial starting position z_{start} for the comparison of the propagation time of the electron pulse. The orange data points refer to all simulation data for this parameter set (the z_{start} values on the horizontal axis only show a part of the total area between the two drift tubes). The positions selected for the ion pulse width definition and electron propagation, respectively, are marked in maroon.

Another global variable is the transfer energy E_{trans} in a.u., which is necessary for the calculation of the azimuth angle Φ_{EII} of the electron impact ionisation part and refers to the potential difference between the virtual cathode of an EBIS and the first drift tube voltage. In figure 2.4 a scheme of the spatial coordinates of the ion momenta can be seen to visualise the different quantities while the beam axis is z and the momentum p_i refers to the input momentum of the electron impact ionisation part or the Maxwell Boltzmann one. For the calculation of the velocity parts in the two before mentioned cases, the same formulas are used but with different input data and different definition of the elevation angle Φ_i, where $i = EII, MB$.

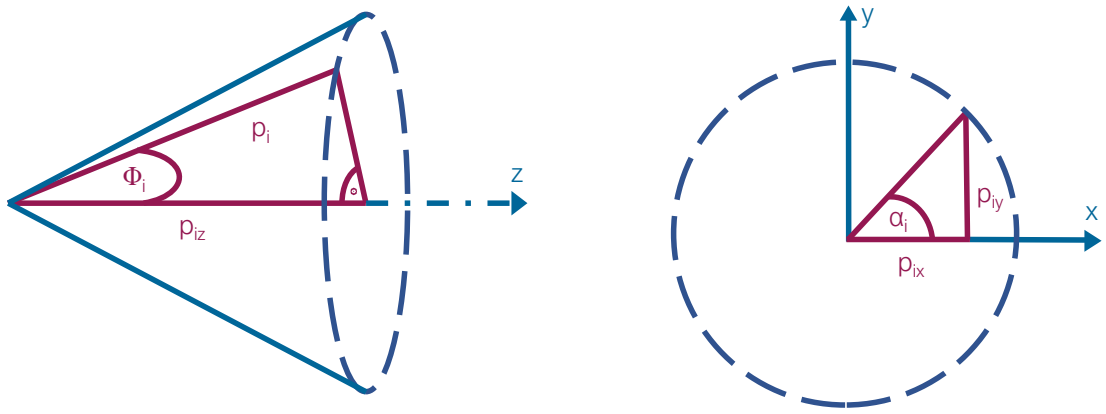

(a) Cone view. (b) View perpendicular to beam axis.

Figure 2.4: Spatial coordinates and angles for the definition of the ion's flying conditions in table 2.2. For more information refer to the the detailed description in the text.

The different Cartesian coordinates are defined referring to table 2.2 as

$$\vec{p}_i = \begin{cases} p_{ix} = p_i \cdot \sin(\Phi_i) \cdot \cos(\alpha_i) \\ p_{iy} = p_i \cdot \sin(\Phi_i) \cdot \sin(\alpha_i) \\ p_{iz} = p_i \cdot \cos(\Phi_i) \end{cases} \tag{2.8}$$

with $i = EII, MB$.

Regarding the velocity part for the temperature the Maxwell Boltzmann distribution f_{MB} generally is given by

$$f_{MB}(v) = 4\pi \left(\frac{m}{2\pi k_B T}\right)^{3/2} \cdot v^2 \cdot e^{-\left(\frac{mv^2}{2k_B T}\right)}. \tag{2.9}$$

Using the Maxwell Boltzmann distribution the velocity direction is isotropic. So, the momentum contributions for an ion are selected from randomly distributed momenta generated with the input of a Maxwell Boltzmann velocity distribution for the desired temperature T. Here, the following temperatures are used: room temperature 300 K, liquid nitrogen temperature 77 K and cryogenic temperatures of 10, 1, 0.5 and 0.01 K. The simulations performed with T = 10 mK can additionally be compared to results from Breuers *et al.* [26]. Figure 2.5 shows the Maxwell Boltzmann distribution in dependence of the velocity for hydrogen for four of the above-mentioned temperatures.

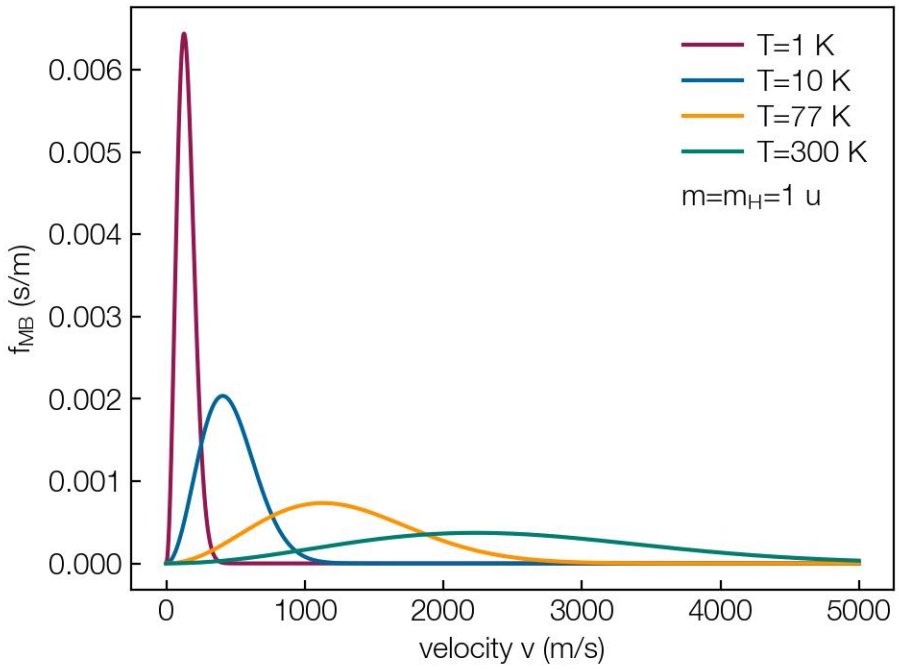

Figure 2.5: Temperature dependence of the velocity distribution for hydrogen with a mass of $m = 1\,u$.

Besides the absolute value of the velocity, angles for the MB part have to be introduced. Both angles are randomly chosen between $\Phi_{MB} = [0,\pi]\,rad$ and $\alpha_{MB} = [0,2\pi]\,rad$, because there is no preferred direction of the ion's momentum due to isotropy in space as mentioned above.
In contrast to the temperature contribution, the part for the electron impact ionisation is more complex. By calculating the ion velocity the azimuthal angle α_{EII} is again randomly distributed in the range of $[0,2\pi]\,rad$. But the elevation angle Φ_{EII} differs in complexity from Φ_{MB} due to the three-body problem of an electron impact ionisation (cf. section 1.1), with the ion being the collision partner of interest in this thesis. When an electron emitted from the cathode hits a hydrogen atom, the path of the scattered electron is deflected not very strongly (cf. figure 1.4) because of a low cross section for high scattering angles. This can also be seen in figure 2.6. As discussed in section 1.1, this leads to a preferred ion recoil momentum perpendicular to the electron beam direction and small overall transferred momenta ($\lesssim 1\,a.u.$).

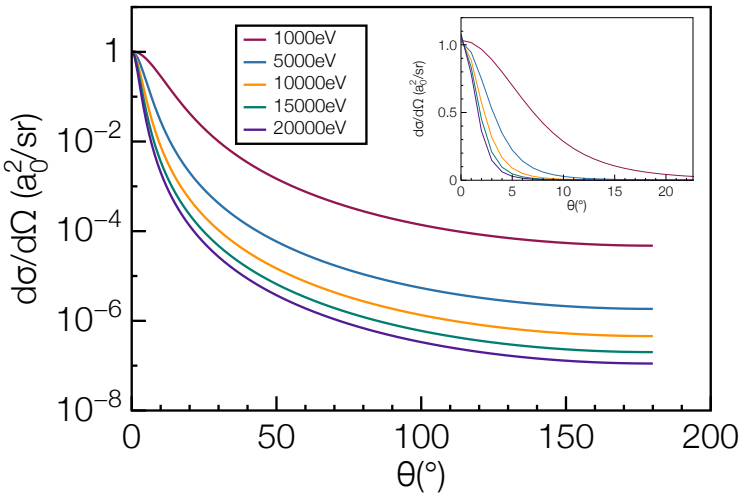

Figure 2.6: Differential cross section in dependence of the scattering angle θ of the electron for a inelastic electron impact ionisation process for different kinetic energies. Data is taken from [36].

In contrast, the ion recoil angle Φ_{EII} mostly directs in the direction perpendicular to the beam axis (cf. figure 1.5). While the data for the EII momenta originate from an inelastic three-body scattering process, the following calculation of the the recoil (elevation) angle Φ_{EII} for every simulated ion is based on an elastic two-body scattering as a maximum estimate and is calculated directly within the LUA script. The calculation of the recoil angle Φ_{EII} according to [37] starts with the momentum definition out of the kinetic energy

$$\mathrm{p_{EII}} = \sqrt{2\mathrm{m_{ion}}\mathrm{E_{trans}}} \tag{2.10}$$

where for the kinetic energy, the energy transfer $\mathrm{E_{trans}}$ is used. The ion mass is represented by $\mathrm{m_{ion}}$ and the momentum by $\mathrm{p_{EII}}$. The energy transferred in an elastic scattering process is defined by

$$\mathrm{E_{trans}} = \gamma \mathrm{E_{proj}} \sin^2 \frac{\theta}{2} \tag{2.11}$$

where the energy for the projectile $\mathrm{E_{proj}}$ refers to the initial energy of the incoming electrons. The energy transfer factor γ uses the projectile and target mass $\mathrm{m_e}$ and $\mathrm{m_{ion}}$, respectively,

$$\gamma = \frac{4\mathrm{m_e}\mathrm{m_{ion}}}{(\mathrm{m_e} + \mathrm{m_{ion}})^2} \tag{2.12}$$

for the ionisation process regarded within this thesis (cf. equation 1.3, replacing A by atomic hydrogen H). After rewriting and inserting equation 2.11 and 2.12 in equation 2.10 an expression for the electron scattering angle θ can be defined. With the relation between scattering and recoil angle

$$\Phi_{\mathrm{EII}} = \frac{\pi - \theta}{2} \tag{2.13}$$

the recoil angle Φ can be finally calculated as

$$\Phi_{EII} = \frac{\pi - 2 \cdot \arcsin\left(\frac{p_{EII}}{\sqrt{2m\gamma E_{proj}}}\right)}{2} \tag{2.14}$$

This relation can be easily implemented in the LUA script as a starting condition for the particles in the SIMION simulation program.

Inserting all mentioned momenta and angles in equation 2.3, the velocity vector for a single ion can finally be defined as

$$\vec{v} = \begin{cases} v_x = \frac{\vec{p}_{x,EII}}{m_{ion}} + \frac{\vec{p}_{x,MB}}{m_{ion}} \\ v_y = \frac{\vec{p}_{y,EII}}{m_{ion}} + \frac{\vec{p}_{y,MB}}{m_{ion}} \\ v_z = \frac{\vec{p}_{z,EII}}{m_{ion}} + \frac{\vec{p}_{z,MB}}{m_{ion}} \end{cases} \tag{2.15}$$

Converting the different contributions of $\vec{v}$ to mm/μs for the usage within SIMION, this calculation can be performed for the desired number of particles by looping over the demanded number of particles.

Recording the ions

In a next step it needs to be defined, which data should be recorded during the simulation. Therefore, the desired physical quantities can be chosen within SIMION. Of great importance is the ions' recording position. SIMION allows to set up a plane in the geometry, where data will be recorded for each particle passing the plane. Regarding the dimensions of the EBIS, the two most important recording positions are right before the extraction unit ($z = 40\,mm$) and at the end of the simulation volume ($z = 143\,mm$). The first z position is interesting because the flight path of the ions is reduced in this case possibly influencing the calculated ion pulse width. Figure 2.7 guides through the different recording positions.

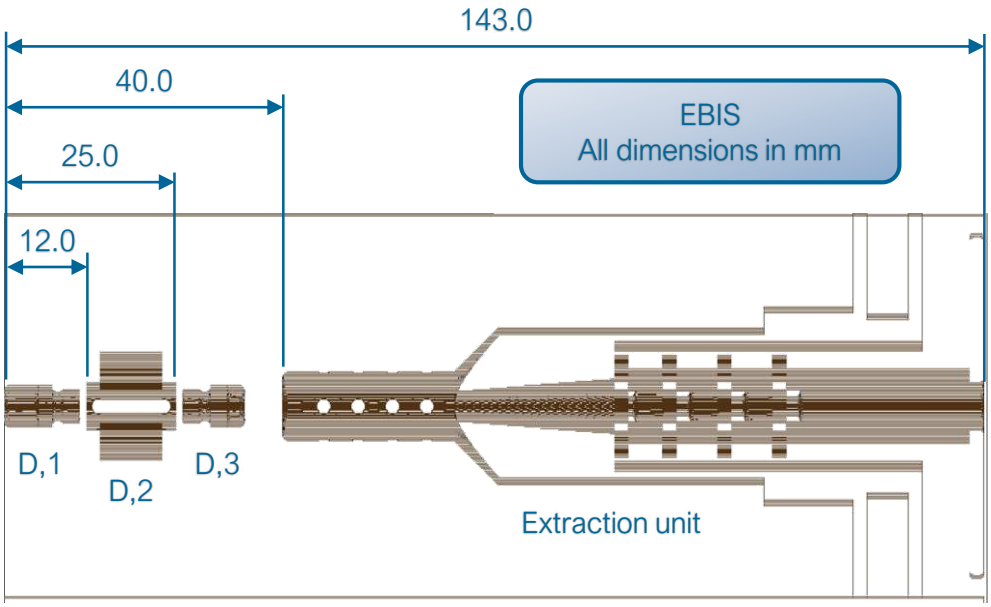

Figure 2.7: Electron Beam Ion Source scheme in the ion trajectory simulation program SIMION including marked z positions.

Flying the ions

To generate the ion trajectories the simulation process has to be started. With a number of particles between 10,000 and 100,000, the simulation process lasts for some minutes. Afterwards the collected data can be evaluated. In the following, the procedure of the data evaluation is presented.

2.3 Data analysis with Python

The data evaluation in this thesis is done in the programming language Python including the data processing, filtering and calculations. The main objective is the determination of the ion pulse width ΔTOF of an ion pulse created and filtered in a similar way as it will be in an experiment. In a laboratory, two curved electrostatic electrodes in a parallel arrangement with an aperture at the end are used to filter ions in a specific energy window. To define the energy range and also the energy resolution $\frac{\Delta E}{E}$ specific voltages and a corresponding aperture need to be used. The voltage is applied in such a way that only the ions with the desired energy can pass the filter.
The energy resolution $\frac{\Delta E}{E}$ according to the project's requirements for such an energy filter lies between 10^{-3} and 10^{-4} , with

$$\Delta E = E_{max} - E_{min}. \tag{2.16}$$

E_{max} and E_{min}, respectively, define the maximum and minimum energy value for the energy filter (see two blue lines in the left part of figure 2.8). E is defined as the energy value in the middle of the energy window

$$E = E_{min} + \frac{\Delta E}{2}. \tag{2.17}$$

In my case, this energy filtering was done in a Python script. ΔE has to be adapted for the ion pulse width calculation according to the maximum energy the ions receive through the drift tube voltage. To remain in the necessary energy resolution range, ΔE lies between a few eV and a few ten eV. For the performed simulations, this energy window is selected manually.

For the ion pulse width ΔTOF calculation with Python all parameters (E, TOF, spatial positions z, etc.) lying between E_{min} and E_{max} are saved separately. With this filtered data a histogram is generated in a next step (see blue bars in right part of figure 2.8, for better visualisation the x axis shows the relative TOF converted into ps). After the calculation of the histogram, the TOF data is fitted with a Gaussian function g(x) (see maroon function in right part of figure 2.8)

$$g(x) = \frac{1}{\sigma \cdot \sqrt{2\pi}} \cdot e^{-\frac{1}{2} \cdot \left(\frac{x-\mu}{\sigma}\right)^2}, \tag{2.18}$$

with the standard deviation σ, the mean μ and x are referred to the filtered TOF values in this thesis. With the help of the Gaussian function the full width at half maximum (FWHM) can be calculated. The FWHM of the Gaussian finally defines the ion pulse width ΔTOF

$$FWHM = 2 \cdot \sqrt{2 \cdot \ln(2)} \cdot \sigma \stackrel{!}{=} \Delta TOF. \tag{2.19}$$

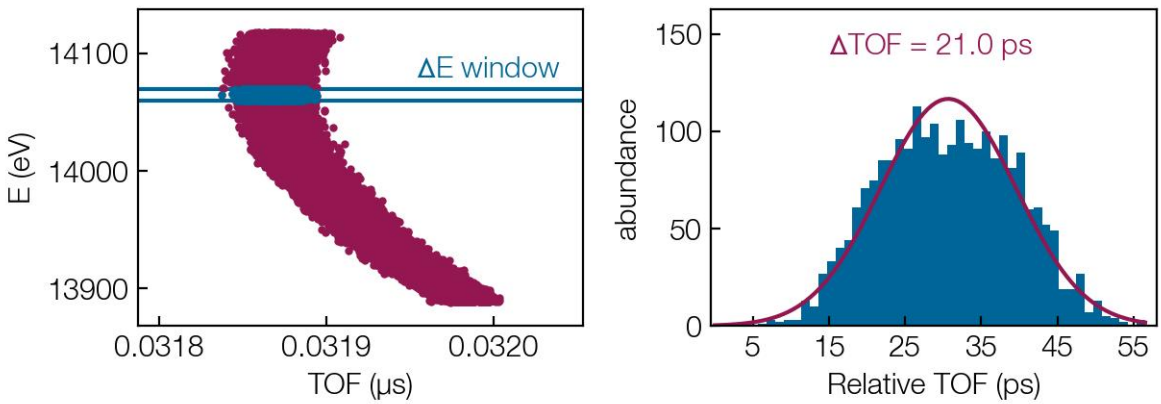

Figure 2.8: Energy versus time of flight graph and ion pulse width definition. Left: Selecting a the kinetic energy window ΔE, ions are taken into account for the pulse width calculation (marked in blue). Right: With the filtered TOF data an histogram is plotted to visualise the abundance of ions within ΔE. The full width at half maximum of the fitted Gaussian defines the ion pulse width ΔTOF.

2.4 Inaccuracies in presented methods

2.4.1 Grid cell size comparison

In section 2.2 the processing of the EBIS geometry with the SL Tools sub-program is discussed. This section addresses the difficulty of the different grid meshes, which can be used for the simulation volume. Within this thesis different geometry configurations are used, which will be explained in detail in section 3.1 (cf. table 3.1). For one setup (including the first and the third drift tube only) simulations are made with different grid cell sizes. For further variation of the geometry, the same grid sizes are used. To receive some insight how the grid size influences the resulting ion pulse width, a CAD drawing of the geometry G_{cut} shown in figure 2.9 is used where the simulation volume is minimised in terms of removing the extraction unit.

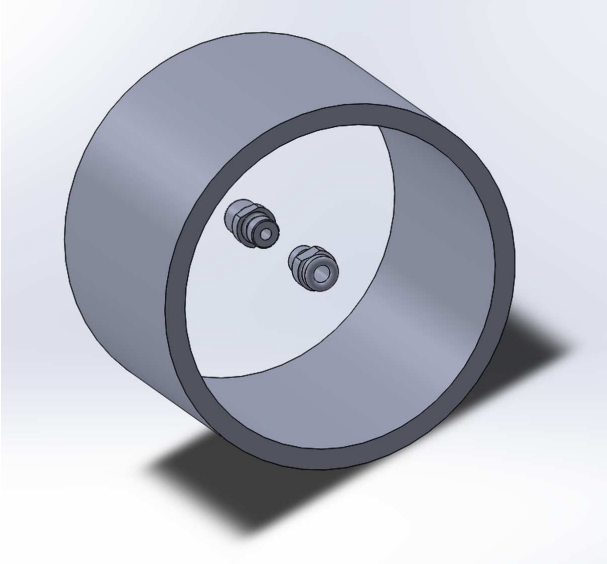

Figure 2.9: CAD drawing without extraction unit to minimise the volume and maximise the spatial resolution.

This minimisation allows to improve the resolution of the total grid (see table 2.3). Nevertheless, this finer grid definition is limited because the smaller the single grid cells are, the larger the amount of disk space needed for the simulation process. In addition, the time necessary for the refining process increases severely.

Table 2.3: Definition of grid cell size for the comparison of different grid resolutions.

grid number	G0	G1	G_{cut}
Δx	0.2 mm	0.1 mm	0.08 mm
Δy	0.2 mm	0.1 mm	0.08 mm
Δz	0.01 mm	0.02 mm	0.015 mm

For the comparison of G0 and G1, where the resolution in Δx and Δy was increased at the cost of the resolution in Δz, I used a set of four parameters simulated for both geometries. In general, the calculated error in the ion pulse width lies between 1 and 4 %. Only in one case a discrepancy of approximately 16 % was found.
The grid definitions also influence the symmetries of the problem. Solids that may have had a cylindrical symmetry in the original CAD drawing are not said to maintain this symmetry when being transformed in a voxel-based model. This also entails another problem as the beam needs to be centred for each voxel geometry and sometimes even in a not completely symmetrical geometry. This may lead to a deflection of the ions into particular directions. This effect is displayed in figure 2.10 where the ions started in a volume centred around (x,y) = (0,0) and clearly were deflected to positive x and y values due to a non-perfect symmetry of the geometry around (0,0).

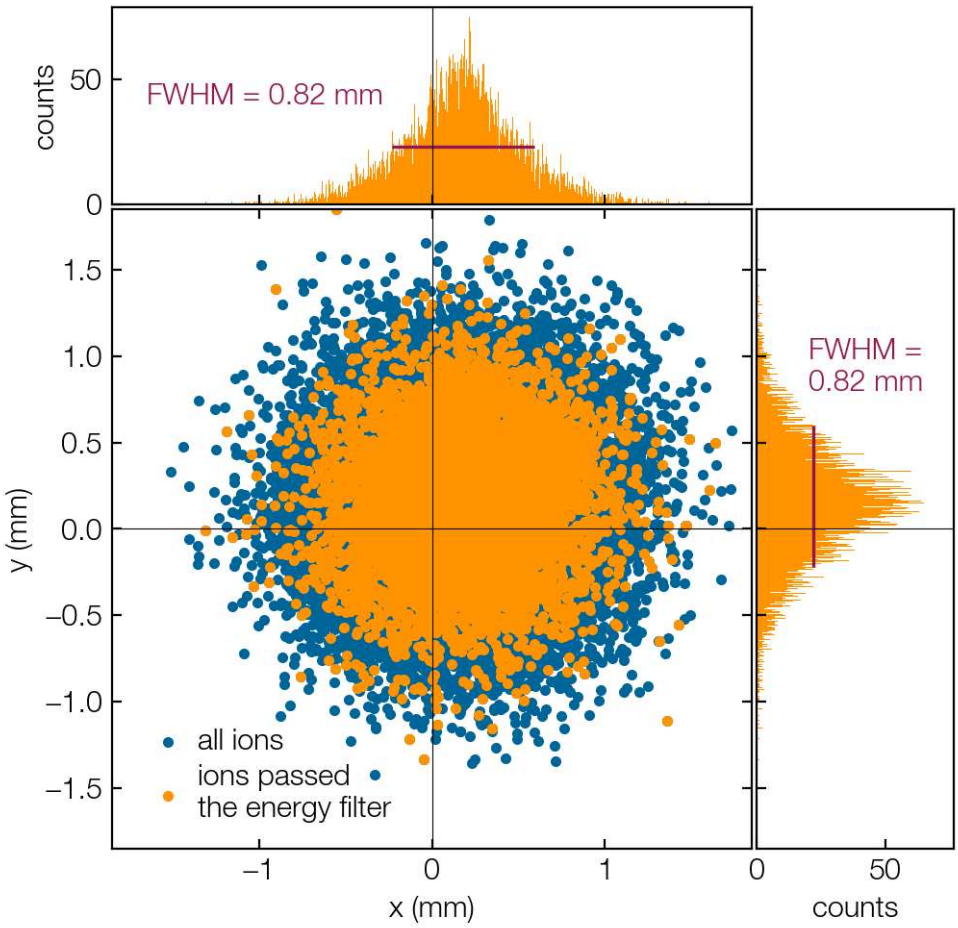

Figure 2.10: Radial ion beam profile. The data is shown for all ions marked in blue, as well as for the energy selected ions that passed the energy filter in orange.

Regarding ΔTOF I find a total maximum relative deviation of the ion pulse width of 12-33 % by comparing G_{cut} and G0/G1. It has to be mentioned that for the same simulation

parameters the ion pulse width is higher within G_{cut}. I assume here that due to an increased resolution the ion trajectories can be calculated more precisely, especially at the point of origin of the ions leading to higher values for the ion pulse width.

Thus, it can be concluded that the calculated ion pulse width may vary in a few tens of percent in total including the two above-mentioned inaccuracies. Simulations presented in chapter 3 were performed using a grid with $\Delta x = 0.1\,\text{mm}$, $\Delta y = 0.1\,\text{mm}$ and $\Delta z = 0.02\,\text{mm}$ ($\hat{=}$ G1).

2.4.2 Numerical discrepancies in ion pulse width calculation

In the course of this thesis the data selected for the calculation of the ion pulse width is defined by the energy window $\Delta E = E_{max} - E_{min}$. Within the Python code, the window is defined by the value for the energy E_{min}. During the data evaluation process I varied E_{min} for the filter manually to achieve a minimum pulse width ΔTOF.
Nevertheless, it was of interest to verify the choice of the selected energy window in the end. Therefore, a separate numerical code was written in Python to calculate the ion pulse width for a set of energy windows (cf. figure 2.8, left: not only calculating ΔTOF for one energy window ΔE (blue) but for all (red) simulated data). The result of the code is the optimum value E_{min} to filter data within the according energy window and calculating the minimum ΔTOF for a given energy resolution. An analysis of the variation of ion pulse width ΔTOF in dependence of the energy E_{min} for the energy resolution values $\frac{\Delta E}{E} = \{10^{-3}, 5 \cdot 10^{-4}, 10^{-4}\}$ is shown in figure 2.11.

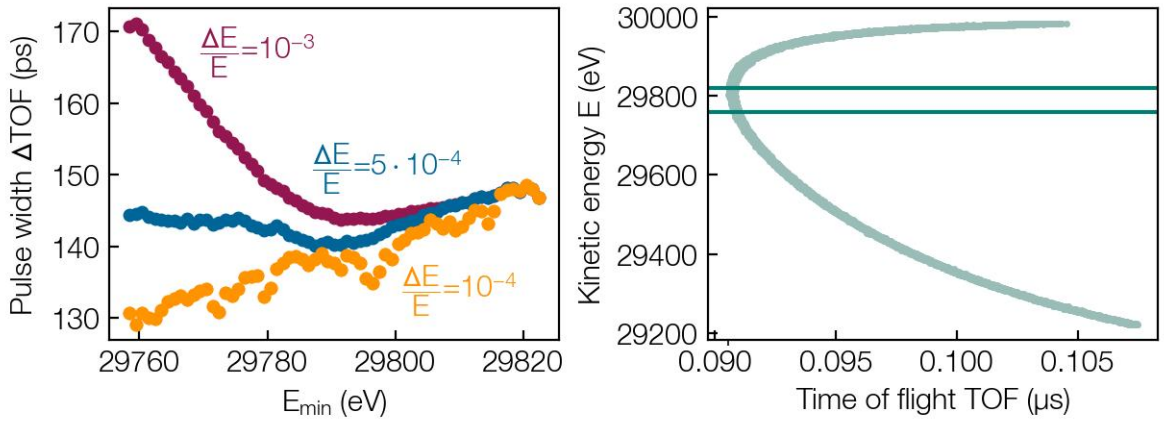

Figure 2.11: Left: The ion pulse width ΔTOF as a function of the minimum energy E_{min} of the energy filter for three different energy resolutions. Right: The kinetic energy versus time of flight with horizontal lines indicating the energy range for the left plot for comparison. The data is calculated using a geometry with the first and second drift tube in a distance of $a_{D,1\text{-}D,2} = 1\,\text{mm}$ and with $U_{D,1} = 30\,\text{kV}$ and $U_{D,2} = 29\,\text{kV}$ applied. The temperature is set to $T = 300\,\text{K}$ and the ions are recorded at $z = 143\,\text{mm}$.

All three curves are calculated with the same original statistics of $5 \cdot 10^4$ ions. The right part of figure 2.11 shows the corresponding full energy versus TOF plot. The two horizontal lines mark the energy range ([29760,29820] eV) selected for the energy resolution variation in the left part of the figure.
A higher energy resolution value $\frac{\Delta E}{E}$ yields in more particles inside the energy window and furthermore more particles available for the ion pulse width calculation. Accordingly, the variation of the energy E_{min} leads to higher discrepancies of ΔTOF for lower $\frac{\Delta E}{E}$ values. Going to higher energies E_{min} the pulse widths seem to match for the different energy resolution values. Due to the fact that all three curves are calculated with $5 \cdot 10^4$ ions, it has to be mentioned that for an energy resolution of $\frac{\Delta E}{E} = 10^{-4}$ the fluctuations rise (see orange curve in figure 2.11). A minimum of the pulse width ΔTOF can be seen between 29780 and 27800 eV in this case referring to a starting position of the ions right after the first drift tube. For a minimum ΔTOF, the estimated error is calculated in this range only (see below).
The maximum error for the ion pulse width is determined by the difference of the mean ΔTOF value for $\frac{\Delta E}{E} = 10^{-3}$ (of red curve in figure 2.11) and $\frac{\Delta E}{E} = 10^{-4}$ (of orange curve) for E_{min} divided by the maximum of E_{min}:

$$\text{error}(\Delta\text{TOF}) = \frac{144.99\,\text{ps} - 137.62\,\text{ps}}{144.99\,\text{ps}} = \frac{7.37\,\text{ps}}{144.99\,\text{ps}} \approx 0.0508 \,\hat{=} 5.1\,\% \tag{2.20}$$

Therefore, the filtering with different energy windows $\frac{\Delta E}{E} = \{10^{-3},\ 10^{-4}\}$ will result in a maximum error for the ion pulse width ΔTOF of approximately 5 %, when the window is chosen properly.

Summarising the discrepancies in ΔTOF regarding the grid comparison on the one hand (two contributions) and the numerical energy window selection on the other hand, a superposition of these effects can lead to a maximum deviation in pulse length of approximately

$$\text{error}(\Delta\text{TOF})_{\text{max,total}} = \sqrt{4^2 + 33^2 + 5^2} \approx 33.6\,\%. \tag{2.21}$$

3 Results and Discussion

In this chapter, the results of the simulations performed in the course of this thesis are presented. Analysis of geometry setups and simulations of the ion pulse width are the main objectives. The subsequent sections cover the variation of the following parameters to investigate the ion pulse width and minimise it for future experiments within the time4ions project:

1. Simulation geometry
2. Ions' recording position z
3. Drift tube voltage $U_{D,i}$
4. Temperature T
5. Electric field $\frac{dU}{dz}$
6. Extraction voltage

The goal is a pulse length of 1 ps. In the end, an optimised ion pulse width for a specific parameter constellation is simulated and the results are discussed.

3.1 Analysis in drift tube configuration and positioning

As mentioned in section 1.2 a commercial EBIS following the design of a DREEBIT EBIS [32] includes, *inter alia*, three drift tubes. The EBIS concept is used here because it is an established ion source for highly charged ions. Because the time4ions project does not aim for a generation of highly charged ions, the source is adapted in terms of the drift tube section to fulfil the desired physical and technical requirements. With the original operating principle including three drift tubes and applying voltage to them according to figure 1.6, highly charged ions can be produced. Here, only two drift tubes are used to generate a desired electric field for the ions. Because the setup for the time4ions project of course includes adaptations, such a modification of the ion source is motivated and justified (see chapter 1.4). Between the two tubes, a constant electric field implying a linear potential gradient is a requirement and has to be achieved (cf. figure 2.2).
Within SIMION simulations this behaviour has been analysed by recording the kinetic energy at every time step of the simulation duration for different geometries and investigating the development especially for the drift tube section. This method is used here to determine and visualise the kinetic energy of the ions within the EBIS in axial direction (z). In table 3.1 the results for different geometries and two drift tube voltage sets of $U_{D,1} = 30\,\text{kV}$ and 15 kV

are summarised. In a commercially available EBIS from [32] the maximum value for a drift tube voltage is 30 kV. Applying such high voltages, one has to pay attention to the dimensions in the setup and distances between the electrodes in order to avoid electrical discontinuities. Therefore, different geometries are discussed. In the following, these setups are called geometry (G) and enumerated from 1 to 5. The different energy versus z position graphs in the right column of table 3.1 refer to different geometries (G1 - G5) designed with SOLIDWORKS and implemented into SIMION to simulate the ion trajectories.

In this thesis, $a_{D,1\text{-}D,i}$ for $i = 2,3$ determines the distance between the drift tubes 1 and i where the potential gradient is defined in-between. Only the distance between two neighbouring drift tubes is discussed, i.e. $a_{D,1\text{-}D,3}$ is only used for geometries without drift tube 2. The illustration column in table 3.1 guides the eye to distinguish between the used geometries. For simplicity reasons, it only shows the drift tubes without the cylindrical electrode around (cf. figure 2.1).
G1 stands for geometry 1 consisting of the first and third drift tube in a distance of $a_{D,1\text{-}D,3} = 15\,\text{mm}$. In geometry G1 the second drift tube is removed and all spatial dimensions are unchanged with respect to the original EBIS CAD drawing. For geometries G2 and G3 also tubes 1 and 3 are used but, the lengths of the drift tubes are extended inwards. Thus, the distance between the tubes decreases to $a_{D,1\text{-}D,3} = 10\,\text{mm}$ (for G2) and $a_{D,1\text{-}D,3} = 5\,\text{mm}$ (for G3), respectively. Geometry G4 consists of all three drift tubes to compare the energy development of only two drift tubes with the original setup. There, the distances between tubes 1 and 2, $a_{D,1\text{-}D,2}$, and between 2 and 3, $a_{D,2\text{-}D,3}$, are 1 mm. In a last drift tube configuration G5 the third tube is removed and the distance between the first and second tube is $a_{D,1\text{-}D,2} = 1\,\text{mm}$ as for G4.
Normally, one would expect a linear energy dependence between the drift tubes using a gradient of 1 kV/mm, for example. Nevertheless, the cylindrical grounded electrode enclosing the drift tube ensemble effects this dependence because the field lines from outside enhance the given electric field between the tubes and disturb the desired linearity. This means the larger the distance between the drift tubes, the easier for the outer electric field to affect the field on the ion's path. This non-linearity can be seen in table 3.1, and for geometries G1, G2 and G3 for 30 kV also bumps (maroon data curves) appear, marked by 'due to external electric field'. Discussing the difference in ion pulse width ΔTOF of geometries G4 and G5 (cf. table 3.1), it can be seen that a longer drift area in G4 (three drift tubes) results in a higher ΔTOF compared to G5 (two drift tubes). For simulations with $T = 300\,\text{K}$, a field gradient of 1 kV/mm and a recording position of $z = 40\,\text{mm}$, ΔTOF differs in about 20 % for the two geometries

$$\frac{\Delta\text{TOF(G4)} - \Delta\text{TOF(G5)}}{\Delta\text{TOF(G4)}} = \frac{171.7\,\text{ps} - 135.8\,\text{ps}}{171.7\,\text{ps}} = \frac{34.0\,\text{ps}}{171.7\,\text{ps}} \simeq 0.198 \hat{\sim} 20\,\%.$$

Table 3.1: Different drift tube configurations. For every geometry G the summary includes: the drift tube number i, the distance between the drift tubes $a_{D,1\text{-}D,i}$, the applied voltages $U_{D,i}$ for i = 1,2,3, an illustration of the geometry and a graph for the kinetic energy E of the ions in dependence of the axial position z for two voltage sets. The potential gradient is always set to 1 kV/mm. The illustrations do not show the grounded cylindrical electrode (cf. figure 2.1).

	i	$a_{D,1\text{-}D,i}$	$U_{D,1}$	$U_{D,2}$	$U_{D,3}$	illustration	E vs. z
G1	3	15 mm	30 kV	-	15 kV	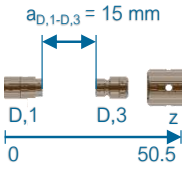	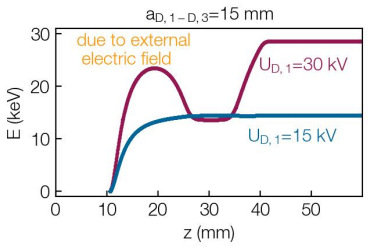
			15 kV	-	0 kV		
G2	3	10 mm	30 kV	-	20 kV	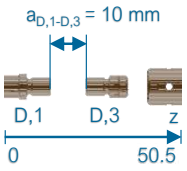	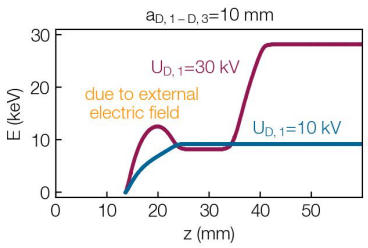
			10 kV	-	0 kV		
G3	3	5 mm	30 kV	-	25 kV	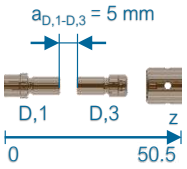	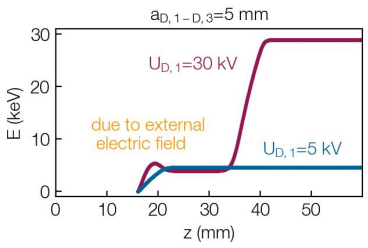
			5 kV	-	0 kV		
G4	2	$a_{D,1\text{-}D,2}$ = 1 mm $a_{D,2\text{-}D,3}$ = 1 mm	30 kV	29 kV	29 kV	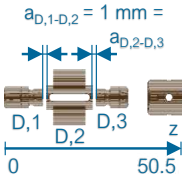	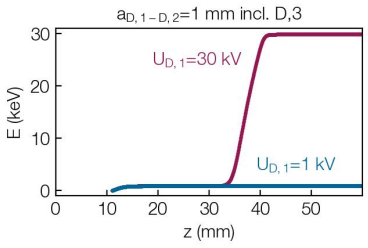
			1 kV	0 kV	0 kV		
G5	2	1 mm	30 kV	29 kV	-	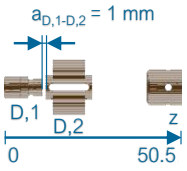	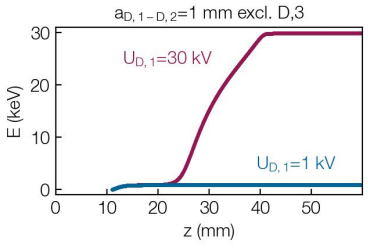
			1 kV	0 kV	-		

3.2 Variation of ions' recording position

As mentioned in section 2.2 the position for data recording can be varied within SIMION. The variation of the z position (collecting data when the ions cross a specific beam axis value plane) is of particular interest for the minimisation of the ion pulse width ΔTOF and thus an optimum setup for the time4ions project.
The question is whether or not there exists a recording position where the ions starting with higher kinetic energies have to cover a longer distance and may then have the same time of flight as ions starting with lower velocities at a later part of the trajectory (cf. two green arrows in figure 2.2). When the TOF of these two ion groups overlaps, a vertical dependence of the kinetic energy as a function of TOF is visible. In the following, the results will be discussed within the variation of the recording position.
Figure 3.1 supports the understanding in terms of definition of the various recording positions. Regarding the EBIS geometry, in figure 3.1 (a) some of the used z positions are marked in the setup. Figure 3.1 (b) shows the different recording positions in an energy E versus z position plot by vertical lines in colour correspondence with the subsequent results.

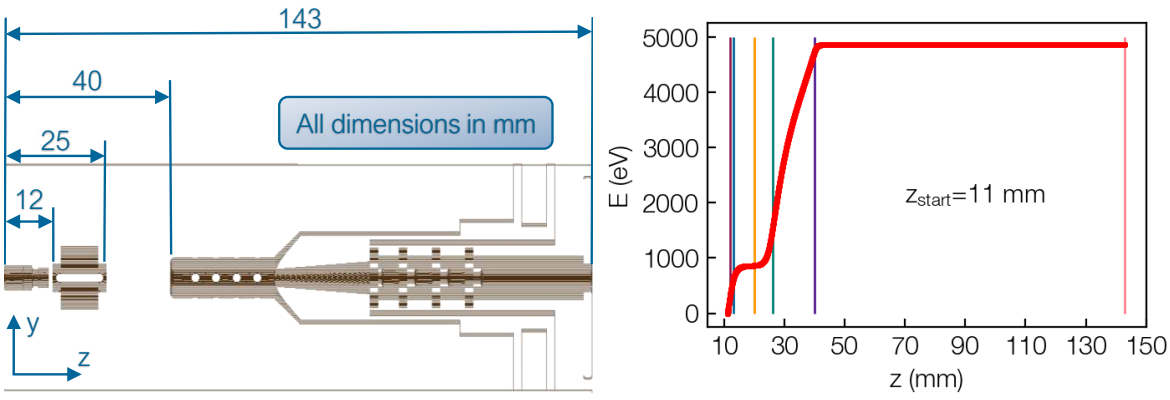

(a) (b)

Figure 3.1: (a) SIMION geometry G5 with two drift tubes in a distance of $a_{D,1\text{-}D,2} = 1\,\text{mm}$ and labels for several z position for better visualisation. (b) Kinetic energy E as a function of the recording z position for the configuration of (a) applying voltages of $U_{D,1} = 5\,\text{kV}$ and $U_{D,2} = 4\,\text{kV}$ to the drift tubes. The ions start to fly at $z_{start} = 11\,\text{mm}$.

For comparison of the recording position dependence, the kinetic energy E is normalised by dividing E by the maximum energy value

$$\text{Normalised E} = \frac{E}{E_{max}}, \tag{3.1}$$

with $E_{max} = qU_{D,1}$, with $q = 1$ for singly charged ions.

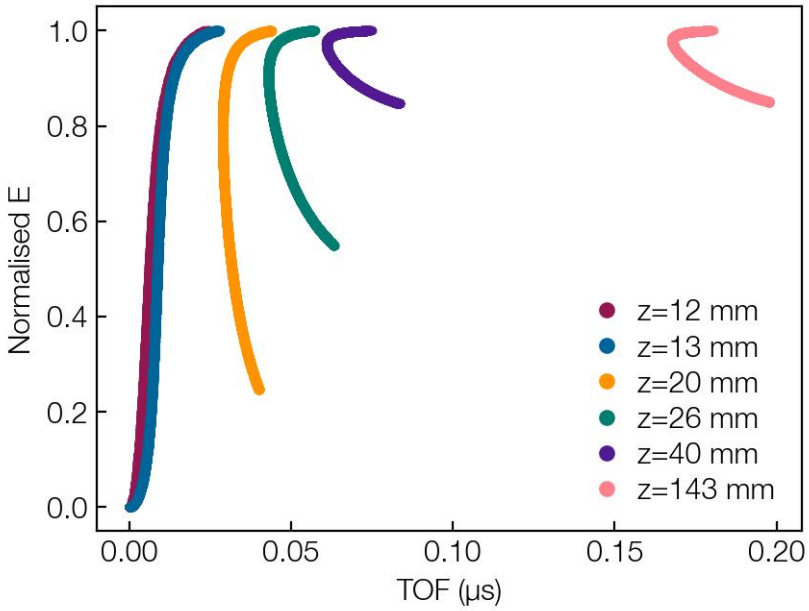

Figure 3.2: Normalised kinetic energy E as a function of the time of flight (TOF) recorded at different positions z using the EBIS geometry of two drift tubes with $U_{D,1} = 5\,kV$ and $U_{D,2} = 4\,kV$ applied in a distance of $a_{D,1\text{-}D,2} = 1\,mm$ ($\hat{=}$ G5, cf. table 3.1).

In figure 3.2 the normalised E is displayed in dependence of the TOF for different recording positions. Comparing the results, it can be seen that it is possible to generate a vertical dependence. For data evaluation, such a steep course results in a larger energy range ΔE from which ions can be filtered afterwards because no unfavourable flanks in the E versus TOF course are emerging. These flanks broaden the pulse width ΔTOF.
As a result of figure 3.2 the ions would need to be selected and subsequently observed inside the second tube between $z = 13\,mm$ (blue) and $20\,mm$ (orange) in this geometry to achieve a vertical dependence. This would entail an observation region of the ions in the drift tube section. For the realisation of an experimental setup to generate ultrashort ion pulses with an EBIS concept this is unhelpful and in addition, obviously technically not feasible.
Nevertheless, a lower axial recording position z always entails a lower flight path and therefore favours a shorter pulse width as well as a lower beam divergence resulting in better conditions for future experiments. For further simulations, the ions' recording position is kept to a low z value, mainly $z = 40\,mm$ (before the extraction unit).

3.3 Different drift tube voltages

In this section the results achieved by varying the voltage of the drift tubes are presented. The maximum voltage for drift tubes in a DREEBIT EBIS [32] is $\sim 30\,kV$.
Varying the drift tube voltage with a constant electric field, the (normalised) energy (E) as a function of the time of flight (TOF) has been analysed. As it can be seen in figure 3.3 for two

recording positions (left: $z = 40\,\text{mm}$; right: $z = 143\,\text{mm}$), a variation in drift tube voltage does entail a change in form of the curves. In figure 3.3 (right) the different voltages for $U_{D,1}$ are marked with the matching colours. Curves in the left part are simulated for the same drift tube voltages and have the same colour code as on the right side.

Generally, the reduction in energy for different voltage sets differs in terms of the various starting positions of the ions. Ions starting closer to the first drift tube refer to the upper right data points in a E versus TOF curve. Applying an electric field of $1\,\text{kV/mm}$ these ions receive a higher kinetic energy in total, after passing the drift tube section (100%). Ions generated near the second tube only receive a fractional amount of energy corresponding to the right bottom edge of an E versus TOF curve (cf. figure 3.3 (left and right)).
Comparing the extremes, this energy reduction is relatively higher for $U_{D,1} = 3\,\text{kV}$ and $U_{D,2} = 2\,\text{kV}$ (maroon) than for 30 and 29 kV (red), for example. In total, the energy declines to $\frac{2\,\text{kV}}{3\,\text{kV}} = 66.6\,\%$ for the first case (maroon), for the second one (red) the ratio yields $\frac{29\,\text{kV}}{30\,\text{kV}} = 96.6\,\%$ of the initial kinetic energy after passing the drift tube section. Figure 3.3 shows cut-outs of the E versus TOF curves, not covering the whole axial starting positions between the two drift tubes leading to a smaller visible decrease in energy as mentioned above.

Varying the drift tube voltage between $U_{D,1} = 3$ and $30\,\text{kV}$ in total, it can be seen that a higher drift tube voltage obviously results in a smaller TOF due to a higher ion velocity. Nevertheless, the main interest is not the total TOF but the relative pulse width ΔTOF the ion beam has after passing an energy filter (cf. section 2.3).

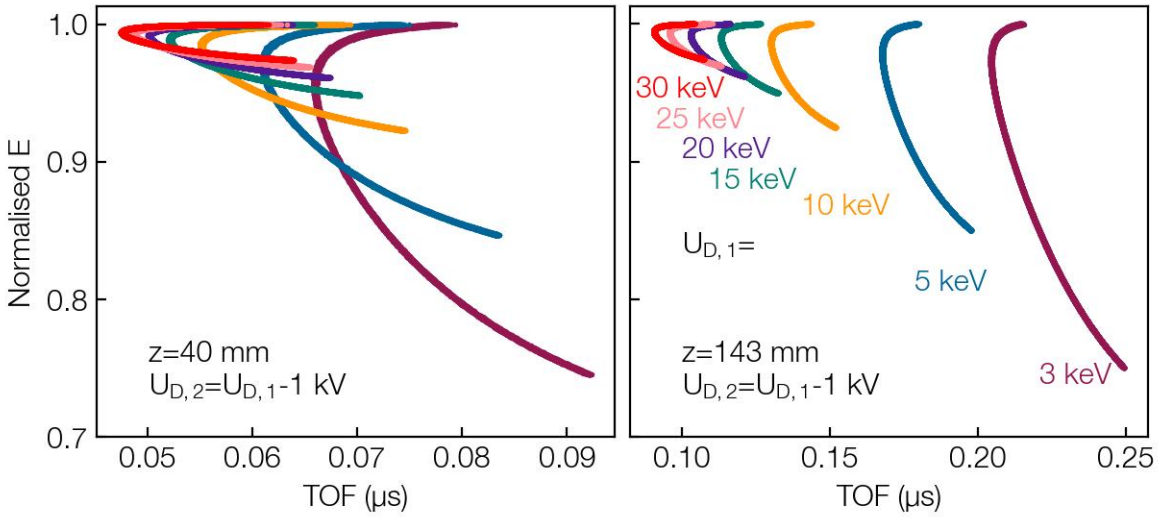

Figure 3.3: Comparison of the normalised particle energy (E) versus the time of flight (TOF) for various drift tube voltages. Using the EBIS geometry G5 with two drift tubes in a distance of $a_{D,1\text{-}D,2} = 1\,\text{mm}$, the potential gradient is set to 1 kV/mm implying that $U_{D,2} = U_{D,1} - 1\,\text{kV}$. Data points are recorded at $z = 40\,\text{mm}$ (left) and $z = 143\,\text{mm}$ (right) corresponding to the entrance of the extraction geometry and to the end of the EBIS volume, respectively (cf. figure 3.1 (a)). The coloured voltages mark $U_{D,1}$ and apply in the same manner for the left part of the figure.

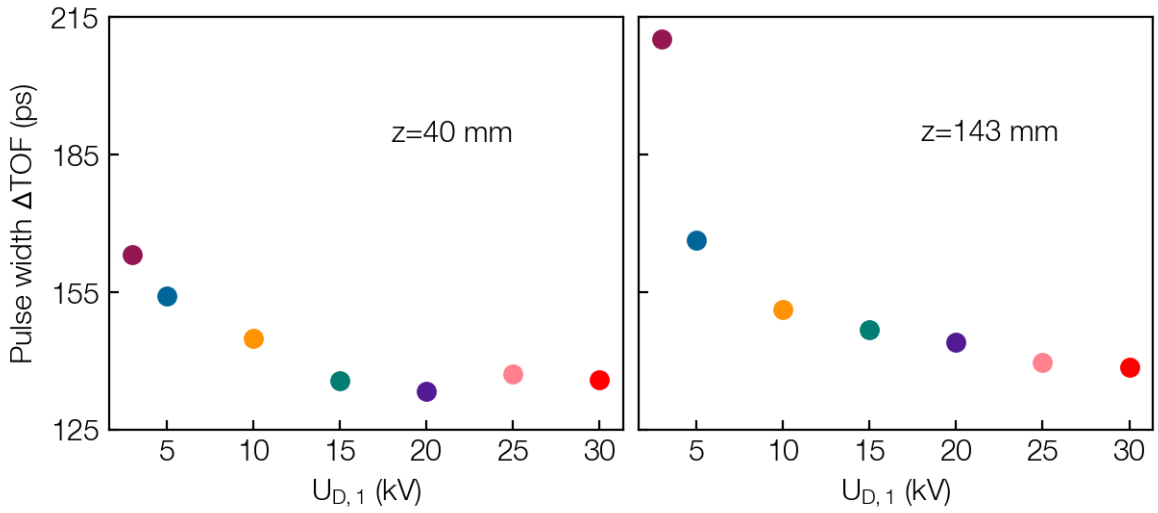

Figure 3.4: Ion pulse width in dependence of the first drift tube voltage $U_{D,1}$ (with $U_{D,2} = U_{D,1} - 1\,\text{kV}$). The data points are generated for a distance $a_{D,1\text{-}D,2} = 1\,\text{mm}$ between the first and the second drift tube ($\hat{=}$ G5). The temperature is kept to 300 K and the recording position is set to $z = 40\,\text{mm}$ (left) and $z = 143\,\text{mm}$ (right). The figure shows the pulse widths corresponding to all curves from figure 3.3 with the same colour code for a direct comparison.

Figure 3.4 depicts the ion pulse widths ΔTOF for the two different recording positions corresponding to figure 3.3, where the drift tube voltages are set between $U_{D,1} = 3$ and 30 kV. Please note that the values for the energy resolution do not have the exact same value but are in the desired range of $\frac{\Delta E}{E} = \{10^{-3}, 10^{-4}\}$ for the calculation of the ion pulse width ΔTOF. Generally, ΔTOF decreases for higher drift tube voltages due to the higher kinetic energy the ions receive when forming. This results in a shorter time of flight and therefore in a lower ΔTOF. The pulse width seems to saturate around 20 - 30 kV. A true explanation for this is provided by the drift tube voltage implying the higher kinetic energy. Important to notice is that the energy filter range is small compared to the range plotted in figure 3.3. Because of the small ΔE value, the general E versus TOF course might not influence the ion pulse width very much.

After presenting results of the drift tube voltage variation, the outcome is discussed in the following. A before-mentioned desired steep E versus TOF course (see section 3.2) for better results does not count here for a minimisation of the ion pulse width ΔTOF. Selecting comparatively small energy ranges for the calculation of ΔTOF out of curves in figure 3.3, a vertical E versus TOF progression is not essential. Due to the error calculations in section 2.4.2, the ion pulse width in figure 3.4 is not constant but also decreases for the high values of $U_{D,1}$ within an error of approximately 5% .

Another advantage besides lower ΔTOF of the resulting high voltage $U_{D,i}$ for the experimental realisation is that higher drift tube voltages lead to a larger permitted energy filter window ΔE for the ion filtering (cf. figure 2.8). This allows a simpler filter design and more ions per pulse.

Within the variation in voltage, the ion pulse width cannot be reduced to the ps range. Therefore, different temperatures in the setup are compared in a next step.

3.4 Temperature variation

An important factor in optimising the ion pulse width might be the gas temperature. Regarding the physics, lower ΔTOF values can be expected for lower temperatures in the simulations. Therefore, a temperature variation has been investigated starting with room temperature 300 K, going over the liquid nitrogen temperature of 77 K down to the mK range including 10 K, 1 K, 500 mK and 10 mK (for comparison with [26]). In figure 3.5 the results of the ion pulse width ΔTOF are presented in dependence of the temperature (T) for two different drift tube voltage sets: $U_{D,1} = 15$ and 30 kV and a potential gradient of $\frac{dU}{dz} = 1$ kV/mm (circles). For both voltage sets a decrease in ΔTOF can be seen for lower temperatures. The minimum pulse width using $\frac{dU}{dz} = 1$ kV/mm lies at 5.7 ps for T = 10 mK. Generally, the trend of a lower ΔTOF for higher drift tube voltage found out in the previous section 3.3 can also be proven with the results in figure 3.5 (blue data points at lower values than red ones).

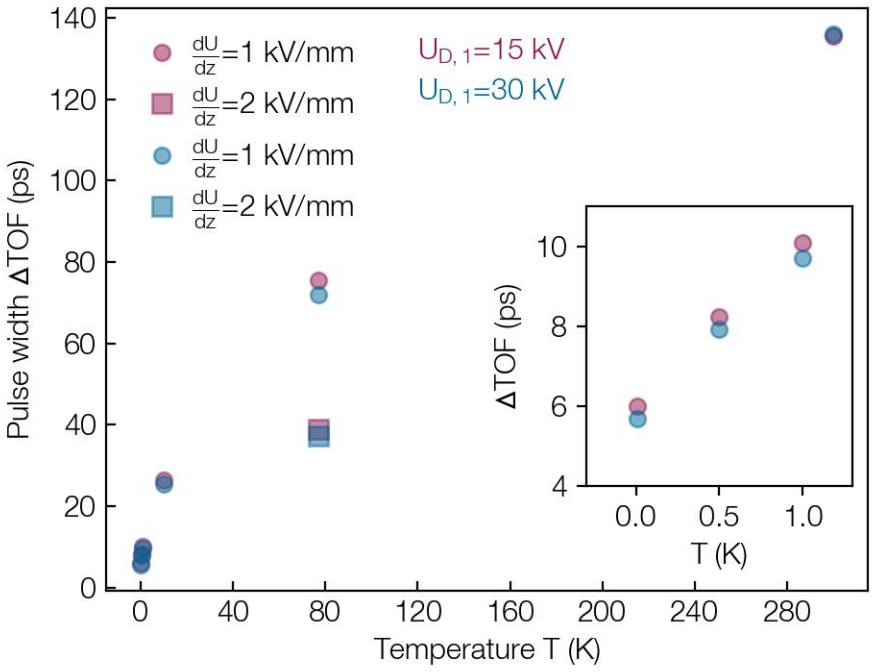

Figure 3.5: Pulse width ΔTOF in dependence of the temperature. The data points are simulated with only the first and second drift tube with a distance of $a_{D,1\text{-}D,2} = 1\,\text{mm}$ and are recorded at $z = 40\,\text{mm}$. The voltages for the drift tubes are set to $U_{D,1} = 15\,\text{kV}$ (maroon data points) and $U_{D,1} = 30\,\text{kV}$ (blue data points), respectively. For visibility the inset again shows the values in the mK region.

Due to a rather difficult feasibility of cryogenic temperatures in the experimental setup (e.g. 10 mK, technically feasible by forming a supersonic jet of gas particles), the potential gradient was raised in a first attempt for $T = 77\,\text{K}$. Using $\frac{dU}{dz} = 2\,\text{kV/mm}$ leads to a decrease in ΔTOF of approximately 50 %. Corresponding data points are marked with squares in figure 3.5. Hence, the influence of the potential gradient will be investigated in the following section. Even though the pulse width can be reduced significantly with lower T, the desired value of 1 ps cannot be achieved with the current setup. In future simulations, and also experiments, a minimised geometry for the generation of short ion pulses will lead to a further decrease in ion pulse width ΔTOF. This includes a reduction in the drift tube length to lower the drift area as well as the spatial dimensions between the electrodes and furthermore the target surface.

3.5 Electric field comparison

When the electron impact ionisation proceeds, ions are generated mostly between the drift tubes. The larger the potential gradient $\frac{dU}{dz}$ between the drift tubes is, the more energy the ions receive depending on their axial starting position: The closer to the first drift tube the ionisation takes place, the higher the energy of the ions will be when arriving at the second

drift tube. Vice versa, ions which are generated close to the second tube gain a lower velocity. However, different flight distances counteract this effect, i.e. ions generated close to the second drift tube exhibit a lower velocity but also need to travel a shorter distance until they reach the second drift tube compared to ions generated close to the first drift tube. Hence, ion pulses with ions created at different positions in-between the drift tubes can still have a short ΔTOF.

The drift tube diameters d_{Drift} in a commercially available EBIS are between 1 - 3 mm. During the preparation of the simulation geometries, the diameters have not been varied. Investigating the influence of the electric field on the ion pulse width, the ratio between the diameters of all drift tubes and the distance $a_{D,1\text{-}D,i}$ with $i = 2,3$ between the two tubes is of great importance. In the following estimation, I used $d_{Drift} = 1$ mm modifying the distance $a_{D,1\text{-}D,i}$ while keeping

$$\frac{d_{Drift}}{a_{D,1\text{-}D,i}} \sim 1. \tag{3.2}$$

Therefore, the variable distance $a_{D,1\text{-}D,i}$ has to be minimised. Based on a tailor-made assembly of an EBIS the distance measures $a_{D,1\text{-}D,2} = 1$ mm. As a result, the geometry G5 with 1 mm distance between the drift tubes is chosen for the potential gradient dependent simulations. To choose experimentally feasible parameters for temperature and voltages, I used the liquid nitrogen temperature $T = 77$ K and $U_{D,1} = 15$ kV. This is a technically stable bias voltage and leads to comparatively small ion pulse widths as well. The results in ΔTOF in dependence of the potential gradient are depicted in figure 3.6.

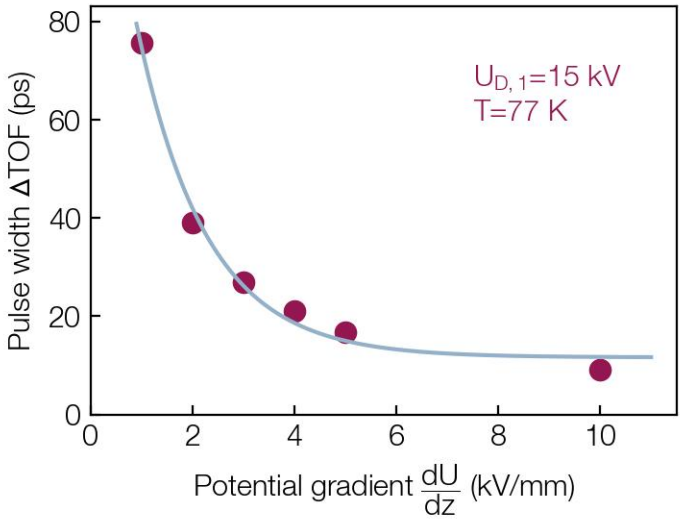

Figure 3.6: Ion pulse width as a function of the potential gradient. The voltage of the first drift tube is set to $U_{D,1} = 15\,kV$ whereby the second one is adjusted in such a way that the potential gradient steadily increases. The electric field comparison is simulated with the first and second drift tube with $a_{D,1\text{-}D,2} = 1\,mm$ ($\hat{=}$ G5) and for a temperature of $T = 77\,K$. The data points are fitted with an exponential function for better visualisation.

In figure 3.6 an exponential decrease of the pulse width with increasing potential gradient is clearly visible. Thus, data points (red) are fitted with an exponential curve (blue). However, the gradient cannot be adjusted arbitrarily high under high vacuum conditions. A feasible range for $\frac{dU}{dz}$ is between 1 and 2 kV/mm, thus data points for a higher potential gradient shall give information about the trend development. However, manufacturing the drift tubes in a way that no sharp edges are present and electro-polishing the surfaces might allow the use of gradients as high as 5 kV/mm. Studies showed breakdown voltages of even up to 50 kV/mm rendering the present assumptions conservative [38].

3.6 Extraction of the ions

This section gives insight in a short investigation of the ion pulse width including non-zero extraction voltage. In the extraction unit of an EBIS, four electrostatic lenses are integrated. The first one represents the extraction lens, the three remaining lenses form an Einzel lens to focus the ion beam, where the first and third lens are generally grounded (cf. section 1.2). Data points in figure 3.7 are simulated with geometry G1, thus the distance between the drift tubes 1 and 3 amounts to 15 mm. This geometry is chosen here because for the ion extraction the distance between the last drift tube and the first extraction lens is significant and should not be too large, which would be the case using G5 as in the previous sections.

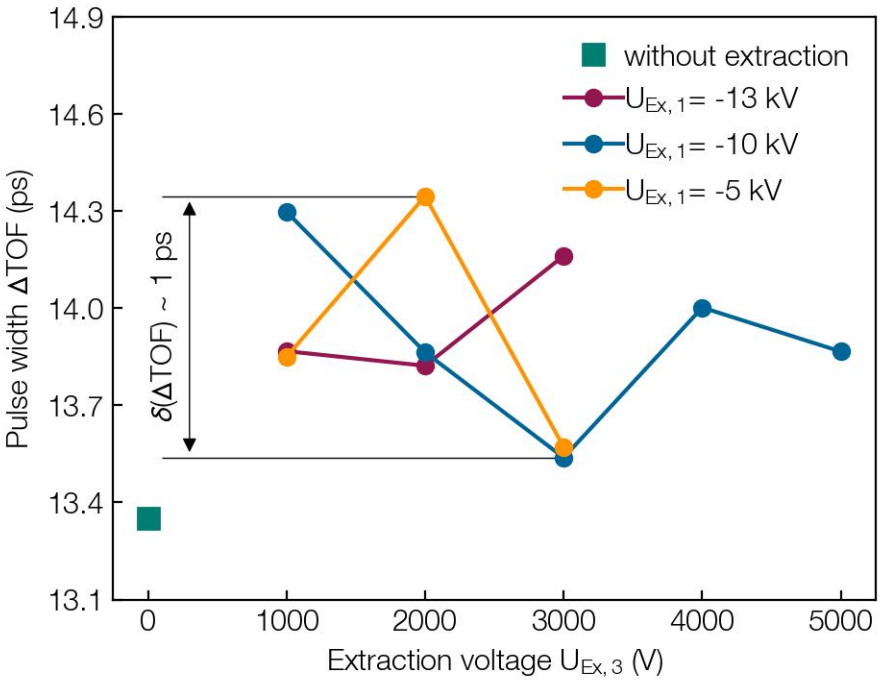

Figure 3.7: Simulation results for the ion pulse width ΔTOF with enabled extraction unit. These data points are simulated with drift tube voltages $U_{D,1} = 30\,kV$ and $U_{D,3} = 15\,kV$ at a temperature of $T = 300\,K$. ΔTOF is calculated at a recording position $z = 143\,mm$, corresponding to the end of the EBIS. The extraction lenses 2 and 4 are set to 0 kV for these simulations. The straight connecting lines are added in this figure to guide the eye.

For this first activation of the extraction, drift tube voltages resulting in low pulse widths ΔTOF are chosen ($U_{D,1} = 30\,kV$ and $U_{D,3} = 15\,kV$). In addition, the temperature, technically easiest to realise, $T = 300\,K$, is adjusted for these simulations. No significant improvements, i.e. no reduction of the pulse width ΔTOF, could be found through activating the extraction geometry, as it can be seen in figure 3.7. Note that the pulse width ΔTOF only varies within $\delta(\Delta TOF) \sim 1\,ps \mathrel{\hat{=}} 7\,\%$ when applying a non-zero extraction voltage.

The ion pulse width is comparatively low in this case because of the large distance between the first and second drift tube. Consequently, field lines are reaching in from the grounded vacuum vessel disturbing the main electric field of the ions. The field distribution inside the drift tubes is therefore not optimised here (cf. see section 3.1). However, the electric field between the third drift tube and the extraction lenses seem to have only little influence on ΔTOF even though it amounts up to almost 6 kV/mm in the simulation. This further justifies the exclusion of the extraction in simulation and experiment to shorten the overall time of flight, but should be investigated in more detail.

3.7 Optimised ion pulse width

In a last step of this thesis, an optimum set of parameters is chosen to simulate a pulse width ΔTOF as low as possible. To sum up, the variable parameters are

- the geometry of the EBIS,
- the voltage for the drift tubes,
- the temperature,
- the ions' recording position and
- the potential gradient.

The biggest limitation currently is the geometry. This means a miniaturised EBIS setup in the future will favour a shorter time of flight and therefore ion pulse width from a current knowledge base even more.
For this simulation the parameters are chosen as follows: Geometry G5 is selected with only the first and second drift tube in a distance of $a_{D,1\text{-}D,2} = 1\,\text{mm}$. This ensures a linear potential gradient between the drift tubes as well as a short drift path for the ions. A voltage of $U_{D,1} = 15\,\text{kV}$ and $U_{D,2} = 13\,\text{kV}$ is applied to the electrodes. It guarantees a rather high but also technically feasible potential gradient of $\frac{dU}{dz} = 2\,\text{kV/mm}$. The temperature is chosen as low as possible to $T = 10\,\text{mK}$, experimentally feasible with a gas jet (cf. sections 1.3 and 3.4). Data is recorded at an axial position of $z = 40\,\text{mm}$ resulting in a shorter total flight path in contrast to recording at the end of the EBIS geometry.
The recorded data from SIMION is evaluated here in two manners: with the manual selection of the energy window and also with the pulse width optimisation code (cf. section 2.4.2). Finally, the manual data analysis leads to an ion pulse width ΔTOF of 4.71 ps (for $\frac{\Delta E}{E} = 10^{-3}$) and 4.18 ps (for $\frac{\Delta E}{E} = 10^{-4}$), respectively. Here, the first ΔTOF should be considered because of low statistics for a higher energy resolution. Besides, the ion pulse width ΔTOF can be minimised down to 4.16 ps using the optimisation code to find the optimum energy window. These optimised results are additionally shown in figure 3.8.
Comparing these two calculated values (ΔE selected manually and with the optimisation code) for the used parameter set, a deviation is noticeable, but the error lies in the range of a few %.
In section 3.4 the potential gradient was varied from 1 kV/mm to 2 kV/mm for $T = 77\,\text{K}$ (cf. figure 3.5) and thus, ΔTOF decreased to about 50 % of the initial pulse width for a higher field of 2 kV/mm. In figure 3.5, the pulse width ΔTOF yields about 6 ps for $T = 10\,\text{mK}$, $U_{D,1} = 15\,\text{kV}$ and 1 kV/mm. For these low gas temperatures, ΔTOF can now be compared with results found for $T = 77\,\text{K}$. It can be estimated that the optimised pulse width ΔTOF (10 mK, 2 kV/mm) does not decrease to about 50 % of the initial pulse width even though simulated with a potential gradient of 2 kV/mm. This means that the temperature dominates

over the potential gradient variation and there is no direct relation in reduction of ΔTOF for the different temperatures when increasing the potential gradient, i.e.,

$$\frac{\Delta\mathrm{TOF}\,(77\,\mathrm{K},\,2\,\mathrm{kV/mm})}{\Delta\mathrm{TOF}\,(77\,\mathrm{K},\,1\,\mathrm{kV/mm})} = \frac{38.9\,\mathrm{ps}}{75.6\,\mathrm{ps}} \hat{=} 50\,\% \neq \frac{\Delta\mathrm{TOF}\,(10\,\mathrm{mK},\,2\,\mathrm{kV/mm})}{\Delta\mathrm{TOF}\,(10\,\mathrm{mK},\,1\,\mathrm{kV/mm})} = \frac{4.2\,\mathrm{ps}}{6.0\,\mathrm{ps}} \hat{=} 70\,\%.$$

Even if the goal for the time4ions project of an ion pulse width of $\Delta\mathrm{TOF} = 1\,\mathrm{ps}$ could indeed not be achieved so far, I think that the deviation is manageable through further improvements of the experimental setup.

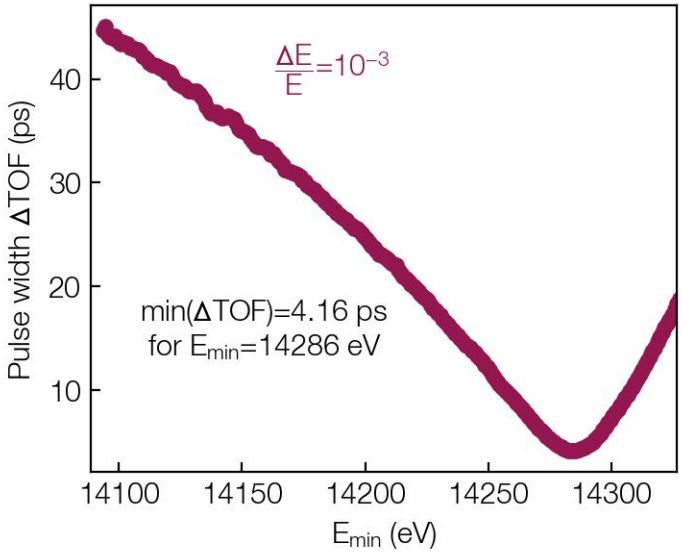

Figure 3.8: Optimisation and calculation of the minimum ion pulse width. ΔTOF is shown in dependence of the minimum energy $\mathrm{E_{min}}$ of the energy filter window for an energy resolution of $\frac{\Delta\mathrm{E}}{\mathrm{E}}$ of 10^{-3}. The ions are simulated with geometry G5 using the first and second drift tube in a distance of $\mathrm{a_{D,1\text{-}D,2}} = 1\,\mathrm{mm}$. Voltages of $\mathrm{U_{D,1}} = 15\,\mathrm{kV}$ and $\mathrm{U_{D,2}} = 13\,\mathrm{kV}$ are applied entailing an electric field of $\frac{\mathrm{dU}}{\mathrm{dz}} = 2\,\mathrm{kV/mm}$. The temperature is set to $\mathrm{T} = 10\,\mathrm{mK}$ and the ions are recorded at $\mathrm{z} = 40\,\mathrm{mm}$.

4 Conclusion and Outlook

Within this thesis, simulations were performed to analyse and optimise an experimental setup to generate ultrafast ion pulses in the near future. Adapting a commercially available electron beam ion source from [32] with the help of SOLIDWORKS, the setup acts as input for simulations performed with the software SIMION. Regarding the particles' flying conditions, an effort was made by calculating the ion velocity vectors and therefore introducing a superposition of the momentum imprinted by an electron impact ionisation process and the Maxwell Boltzmann distribution; the latter includes the temperature within the simulated setup. The recorded data was then evaluated using a Python script to recreate an experimental energy filter (electrostatic analyser) and to determine the ion pulse width ΔTOF. It was of interest to vary different parameters in a way to reduce ΔTOF to the goal of 1 ps.

The simulation results presented in chapter 3 show that it is necessary to combine various optimised parameters such as spatial dimensions, recording positions, drift tube voltages, temperature and field gradient to minimise the ion pulse width.

Using different simulation geometries, I figured out that when reducing the number of drift tubes from three to two (e.g. removing the second one), comparatively large distances ($a_{D,1\text{-}D,3} = 15$, 10 or 5 mm for G1, G2 and G3) result in an enhancement of the local electric field the ions experience. The outer field lines from the grounded cylindrical electrode indeed alter the electric field and so, the desired linear potential gradient is disturbed (cf. table 3.1). Therefore, the distances between the tubes are minimised using only the first and second drift tube in a distance of $a_{D,1\text{-}D,2} = 1$ mm, resulting in a stable electric field. In addition, the drift path (corresponding to the length of the tubes) has to be kept low in order to minimise the ion pulse width in the end.

Varying the ions' recording position, a vertical dependence in the energy as a function of the time of flight is generally favourable, because it leads to a wider energy range ΔE from which the ions can be selected. Nevertheless, the recording position has to be technically feasible (not within the drift tube unit) but should be chosen to the smallest possible value to guarantee a short flight path. In section 3.3 I showed that higher drift tube voltages lead to a lower pulse width due to a higher kinetic energy of the ions.

I also analysed that, independent from the drift tube voltage, lower temperatures lead to smaller pulse widths. ΔTOF has been simulated for different temperatures: 300 K, 77 K, 10 K, 1 K, 500 mK and 10 mK. The potential gradient $\frac{dU}{dz}$ was kept to 1 kV/mm for the simulations in the beginning. In a first try, a higher gradient of 2 kV/mm was applied using

$T = 77\,K$. As a strong decrease in ΔTOF with $2\,kV/mm$ was found, the influence of the potential gradient $\frac{dU}{dz}$ has been further investigated resulting in lower ion pulse widths for high gradients (cf. figure 3.6). Even though I am aware of the difficult technical feasibility of high electric fields, I suggest to use the highest possible potential gradient ($\sim 2\,kV/mm$), as it seems most suitable to achieve low pulse widths in future experiments.

To form and focus the ion beam, the extraction unit was included in a few simulations as well. Investigating ΔTOF for different extraction voltages, no improvement of the pulse width could be achieved using the current EBIS geometry and particle definitions. Besides, a total removal of the extraction section is suggested for the time4ions project to reduce flight distances and thus TOFs. In the end, ΔTOF was simulated using an optimised parameter set. We have seen, that even with $T = 10\,mK$ and $\frac{dU}{dz} = 2\,kV/mm$ the pulse width could not be reduced to the desired 1 ps. The minimum value found within this thesis yields approximately 4 ps.

Limitations in the ion pulse generation can be determined regarding the ionisation process. In the used electron impact ionisation, isotropic distribution of the gas particles is assumed. Large ion momenta could be determined due to forward scattering of the impacting electrons, but their cross sections are close to zero (cf. figure 1.3 and figure 1.4). So, most of the ions fly with large recoil angles (cf. figure 1.5) limiting the currently available ion pulse width minimisation. As a further improvement, the electron impact ionisation could be replaced by laser ionisation. Therefore, a generated gas particle jet (e.g. [26]) could be installed such that a laser can be directed onto the gas jet in a way to ensure a forward direction of the ionised particles. This would lead to a minimisation of the ion pulse width in the end.

One has to mention that the geometric dimensions have not been minimised within this thesis. Using a miniaturised simulation geometry by especially reducing the length of drift tubes in axial direction, may help to minimise the ion pulse width even more in order to investigate ultrashort ion-surface interaction processes. In addition, an improvement can be made by including the cathode for the electron generation as well as the magnets in an EBIS. In the course of implementing the cathode in SIMION also the electrons emerging from the cathode and yielding the electron impact ionisation can be directly simulated. This improvement of the simulations would approximate the experimental conditions (later also the electrostatic energy filter could be included in the geometry) and integrate the true physics of the time4ions project even more.

A possible adaptation of the experimental setup was discussed in section 3.6, where the extraction unit is completely removed in order to save flight time and achieve a shorter ion pulse width. If the extraction system would be omitted another opportunity for the setup would be to install only two drift tubes with a short distance in-between and add deflection plates right after the second tube operating as an energy filter and place the target behind the plates.

According to the particle properties, redefining the kinetic energy of the electrons after implementing the cathode could result in an optimised pulse width. In more detail, when specifying the particle properties (see section 2.2) the transfer energy, i.e. the energy the ions start to fly

with, is defined. Until now, it was set to a value related to the voltage of the first drift tube. An approach could be to change this energy by applying high voltage to the cathode. For example, if 15 kV are applied to the first drift tube, the cathode can be biased to 14.95 kV. The acceleration voltage for the electrons released from the cathode is then comparatively low. With a transfer energy of $E = 50\,eV$ the electrons' kinetic energy is closer to the binding energy of the electron in a gas atom leading to larger cross sections for the impact ionisation. It would be interesting to investigate if the pulse width ΔTOF decreases as a result of the lowered transfer energy leading to higher cross sections.
In the end, I think if the above-mentioned results are taken into account, especially a miniaturised setup and the here presented optimised parameters, the desired ion pulse width of 1 ps can be achieved in future simulations and further on in experiments.

Bibliography

[1] M. Nastasi and J.W. Mayer. *Ion implantation and synthesis of materials*. Springer Verlag Berlin Heidelberg, 2006.

[2] A. Wallner, J. Feige, N. Kinoshita, M. Paul, L.K. Fifield, R. Golser, M. Honda, U. Linnemann, H. Matsuzaki, S. Merchel, G. Rugel, S.G. Tims, P. Steier, T. Yamagata, and S.R. Winkler. Recent near-Earth supernovae probed by global deposition of interstellar radioactive 60 Fe. *Nature*, 532(7597):69–72, 2016.

[3] M. Durante and J.S. Loeffler. Charged particles in radiation oncology. *Nature Reviews Clinical Oncology*, 7(1):37–43, 2010.

[4] J. Knaster, A. Moeslang, and T. Muroga. Materials research for fusion. *Nature Physics*, 12(5):424–434, 2016.

[5] E. Gruber, R.A. Wilhelm, R. Pétuya, V. Smejkal, R. Kozubek, A. Hierzenberger, B.C. Bayer, I. Aldazabal, A.K. Kazansky, F. Libisch, A.V. Krasheninnikov, M. Schleberger, S. Facsko, A.G. Borisov, A. Arnau, and F. Aumayr. Ultrafast electronic response of graphene to a strong and localized electric field. *Nature Communications*, 7:13948, 2016.

[6] R.A. Wilhelm, E. Gruber, J. Schwestka, R. Kozubek, T.I. Madeira, J.P. Marques, J. Kobus, A.V. Krasheninnikov, M. Schleberger, and F. Aumayr. Interatomic Coulombic Decay: The Mechanism for Rapid Deexcitation of Hollow Atoms. *Physical Review Letters*, 119(10):103401, 2017.

[7] J. F. Ziegler, M. D. Ziegler, and J. P. Biersack. SRIM - The stopping and range of ions in matter (2010). *Nuclear Instruments and Methods in Physics Research, Section B: Beam Interactions with Materials and Atoms*, 268(11-12):1818–1823, 2010.

[8] L. Bukonte, F. Djurabekova, J. Samela, K. Nordlund, S. A. Norris, and M. J. Aziz. Comparison of molecular dynamics and binary collision approximation simulations for atom displacement analysis. *Nuclear Instruments and Methods in Physics Research, Section B: Beam Interactions with Materials and Atoms*, 297:23–28, 2013.

[9] J. Samela and K. Nordlund. Atomistic simulation of the transition from atomistic to macroscopic cratering. *Physical Review Letters*, 101(2):027601, 2008.

[10] F. Aumayr. Atomare Stoßprozesse. *Lecture Notes*, 2020.

[11] A. Einstein. Über einen die Erzeugung und Verwandlung des Lichtes betreffenden heuristischen Gesichtspunkt. *Annalen der Physik*, 322(6):132–148, 1905.

[12] A. L'Huillier, L. A. Lompre, G. Mainfray, and C. Manus. Multiply charged ions induced by multiphoton absorption in rare gases at 0.53 μm. *Physical Review A*, 27(5):2503–2512, 1983.

[13] R. Moshammer, B. Feuerstein, W. Schmitt, A. Dorn, C. D. Schröter, J. Ullrich, H. Rottke, C. Trump, M. Wittmann, G. Korn, K. Hoffmann, and W. Sandner. Momentum distributions of Ne n+ ions created by an intense ultrashort laser pulse. *Physical Review Letters*, 84(3):447–450, 2000.

[14] V. Hanus, S. Kangaparambil, S. Larimian, M. Dorner-Kirchner, X. Xie, M.S. Schöffler, G.G. Paulus, A. Baltuška, A. Staudte, and M. Kitzler-Zeiler. Experimental Separation of Subcycle Ionization Bursts in Strong-Field Double Ionization of H2. *Physical Review Letters*, 124(10):103201, 2020.

[15] M. Génévriez, J.J. Jureta, P. Defrance, and X. Urbain. Absolute cross section for electron-impact ionization of He(1s2s S 3). *Physical Review A*, 96(1):010701, 2017.

[16] E.D. Donets and V.P. Ovsyannikov. Investigation of ionization of positive ions by electron impact. *Sov. Phys. JETP*, 53(3):466–471, 1981.

[17] B. Lohmann and E. Weigold. Direct measurement of the electron momentum probability distribution in atomic hydrogen. *Physics Letters A*, 86(3):139–141, 1981.

[18] I.E. McCarthy and E. Weigold. Electron momentum spectroscopy of atoms and molecules. *Reports on Progress in Physics*, 54(6):789–879, 1991.

[19] I.E. McCarthy and E. Weigold. (e, 2e) Spectroscopy. *Physics Reports*, 27(6):275–371, 1976.

[20] R. Geller. ECRIS: the electron cyclotron resonance ion sources. *Annu. Rev. Nucl. Part. Sci., vol. 40, p. 15*, 1990.

[21] J. Arianer. The advanced positive heavy ion sources. *Nature*, 1(15):380–380, 1870.

[22] G. Zschornack, M. Kreller, V. P. Ovsyannikov, F. Grossman, U. Kentsch, M. Schmidt, F. Ullmann, and R. Heller. Compact electron beam ion sources/traps: Review and prospects. *Review of Scientific Instruments*, 79(2), 2008.

[23] U. Kentsch, S. Landgraf, G. Zschornack, F. Grossmann, V. P. Ovsyannikov, and F. Ullmann. Dresden EBIT: Results and perspectives. *Review of Scientific Instruments*, 73(2 II):660, 2002.

[24] F.J. Bergmeister, K.P Lieb, and D. Sträter. A nanosecond pulsing system for the cologne FN tandem accelerator. *Nuclear Inst. and Methods in Physics Research, A*, 244(1-2):176–179, 1986.

[25] N. Olsson. A 100 picosecond post-acceleration bunching system at the Studsvik 6 MV Van de Graaff accelerator. *Nuclear Instruments and Methods*, 187(2-3):341–346, 1981.

[26] A. Breuers, M. Herder, P. Kucharczyk, M. Schleberger, K. Sokolowski-Tinten, and A. Wucher. A concept to generate ultrashort ion pulses for pump-probe experiments in the keV energy range. *New Journal of Physics*, 21(5):053017, 2019.

[27] M. Mittendorff, F. Wendler, E. Malic, A. Knorr, M. Orlita, M. Potemski, C. Berger, W.A. De Heer, H. Schneider, M. Helm, and S. Winnerl. Carrier dynamics in Landau-quantized graphene featuring strong Auger scattering. *Nature Physics*, 11(1):75–81, 2015.

[28] M.T. Hassan, J.S. Baskin, B. Liao, and A.H. Zewail. Highoral-resolution electron microscopy for imaging ultrafast electron dynamics. *Nature Photonics*, 11(7):425–430, 2017.

[29] A.H. Zewail. Four-Dimensional Electron Microscopy. *Science*, 328(5975):187–193, 2010.

[30] D.R. Herriott and H.J. Schulte. Folded Optical Delay Lines. *Applied Optics*, 4(8):883, 1965.

[31] SOLIDWORKS. Solid modeling CAD program. Dassault Systemes Solidworks Corporation. *https://www.solidworks.com/*, 15.09.2020, 2020.

[32] DREEBIT. Ion beam technology. *https://www.dreebit-ibt.com/ion-sources.html*, 29.09.2020, 2020.

[33] SIMION. Particle trajectory simulation software. Scientific Instrument Services. *https://www.simion.com/*, 18.09.2020, 2020.

[34] D. Manura and D. Dahl. Simion 8.1 user manual. *Scientific Instrument Services, Inc. Ringoes, NJ 08551*, 2011.

[35] Lua. Programming language. *https://www.lua.org/about.html*, 22.09.2020, 2020.

[36] NIST Standard Reference Database. Electron Elastic-Scattering Cross-Section Database. *https://srdata.nist.gov/SRD64/*, 07.10.2020, 2020.

[37] R.A. Wilhelm. Ion-solid interaction. *Lecture Notes*, 2019.

[38] D.W. Williams and W.T. Williams. Effect of electrode surface finish on electrical breakdown in vacuum. *Journal of Physics D: Applied Physics*, 5(10):1845–1854, 1972.

Danksagung

Nun ist es Zeit, von Herzen Danke zu sagen für die wundervolle Zeit, die ich am Institut für Angewandte Physik erleben durfte. Innerhalb des letzten Jahres durfte ich unglaublich viel neues Wissen erwerben aber auch neue Erfahrungen im Leben einer Physikerin sammeln. Das hat vor allem eines möglich gemacht, die Offenheit und Herzlichkeit, die stets in der Arbeitsgruppe zu spüren ist, all die freundlichen Gespräche untereinander und die hilfreichen wissenschaftlichen Diskussionen.

Allen voran möchte ich dir, Fritz, von Herzen danken, dass du mich in deine Gruppe aufgenommen hast und immer ein offenes Ohr für mich hattest. Danke für deine professionellen Inputs zu meiner Arbeit, aber auch für dein Dasein als Professor, wo du mich von der ersten Minute als Physikstudentin in der Einführungsvorlesung begleitet hast. Ich freue mich sehr, dass ich ein kleiner Teil deiner Gruppe sein durfte.

Lieber Richard, ich kann mich noch gut an unsere Diskussionen zur Optimierung der Startbedingungen im Frühjahr während des Corona-Lockdowns erinnern. Es hat mir großen Spaß gemacht, mit dir an den verschiedenen Details meiner Arbeit zu feilen und mich mit dir auszutauschen. Herzlichen Dank für die Aufnahme in dein time4ions Team. Dein unglaubliches Wissen hat mich von Anfang an fasziniert und auch motiviert nicht aufzuhören, diese Arbeit stets zu verbessern. Es hat mir sehr große Freude gemacht, ganz am Beginn eines so tollen Projektes einen kleinen Beitrag zu leisten. Danke für all dein Feedback, durch das ich ausgesprochen viel neues Wissen sammeln durfte und für all die kleinen Details, auf die du mich aufmerksam gemacht hast. Ich bin fest davon überzeugt, dass du die eine Picosekunde hinbekommst.

Ein riesiges Dankeschön gebührt dir, Anna, eine wahre Freundin, tolle Kollegin und spitzen Korrektur-Leserin. Nachdem wir ja bereits durch einen Großteil unserer Studienzeit gemeinsam gegangen sind, nun auch ein Danke für all deine konstruktiven Inputs, deine Zeit, die du mir geschenkt hast, um gemeinsam zu programmieren, meine Arbeit zu lesen, über Resultate zu diskutieren, auch einfach nur zu plaudern oder ab und zu gemeinsam zu backen. Die Liste könnte ich noch sehr lange fortsetzen, also: Von Herzen Danke, Anna!

Und natürlich möchte ich mich auch bei den anderen aus der Arbeitsgruppe recht herzlich bedanken: Bei Janine für die Frauenpower; bei Reinhard für die Unterstützung bei der Anschaffung eines neuen Rechners für meine Simulationen; bei Gabriel für den time4ions Austausch; bei Waldemar, dem lieben Bürokollegen; bei Paul, Herbert, Georg und Christian für die gemeinsamen Gespräche wissenschaftlicher und alltäglicher Natur; bei Lidija für das

gemeinsame Hinfiebern zur Einreichfrist und die gegenseitigen Erinnerungen; bei Martin für die Einführung in die Hall-Sonde, die angenehmen Gespräche und Freihausführungen und natürlich bei allen anderen, die die Zeit am IAP zu einer ganz besonderen gemacht haben.
Danke auch an meine Lerngruppe, Anna, Gabriel, Martin, Manuel, Johanna, Daniel und Florian, ohne die meine nun endende Studienzeit nicht die selbe gewesen wäre.
Ein riesengroßes Dankeschön möchte ich an meinen lieben Freund, Manuel, richten. Du hast mich in den letzten Jahren und vor allem in den letzten Monaten in meiner Studienzeit begleitet und trotz so mancher langen Lern- und Schreibnächte, warst und bist du immer für mich da. Zu guter Letzt möchte ich mich von ganzem Herzen bei meinen lieben Eltern, meinen drei Brüdern und meinen Großeltern bedanken, dass ihr diese Studienzeit für mich möglich gemacht habt und mich immer unterstützt habt.